Historical Perspective

Interactions of particulate matter and pulmonary surfactant: Implications for human health

Feifei Wang [a,b], Jifang Liu [a,*], Hongbo Zeng [b,*]

[a] *The Fifth Affiliated Hospital, Guangzhou Medical University, Guangzhou, Guangdong 510700, China*
[b] *Department of Chemical and Materials Engineering, University of Alberta, Edmonton, AB T6G 1H9, Canada*

ARTICLE INFO

ABSTRACT

Particulate matter (PM), which is the primary contributor to air pollution, has become a pervasive global health threat. When PM enters into a respiratory tract, the first body tissues to be directly exposed are the cells of respiratory tissues and pulmonary surfactant. Pulmonary surfactant is a pivotal component to modulate surface tension of alveoli during respiration. Many studies have proved that PM would interact with pulmonary surfactant to affect the alveolar activity, and meanwhile, pulmonary surfactant would be adsorbed to the surface of PM to change the toxic effect of PM. This review focuses on recent studies of the interactions between micro/nanoparticles (synthesized and environmental particles) and pulmonary surfactant (natural surfactant and its models), as well as the health effects caused by PM through a few significant aspects, such as surface properties of PM, including size, surface charge, hydrophobicity, shape, chemical nature, etc. Moreover, *in vitro* and *in vivo* studies have shown that PM leads to oxidative stress, inflammatory response, fibrosis, and cancerization in living bodies. By providing a comprehensive picture of PM-surfactant interaction, this review will benefit both researchers for further studies and policy-makers for setting up more appropriate regulations to reduce the adverse effects of PM on public health.

© 2020 Published by Elsevier B.V.

Contents

* Corresponding authors.
  E-mail addresses: yzhbb2012@126.com (J. Liu), hongbo.zeng@ualberta.ca (H. Zeng).

1. Introduction

Nowadays air pollution has become one of the top health killers all around the world [1,2]. The main pollutants contain ozone (O_3), nitrogen dioxide (NO_2), sulfur dioxide (SO_2), and particulate matter (PM) [3]. PM is reported to induce adverse effects on human health after either short-term or long-term exposure. Short-term exposure generally causes acute inflammatory responses in airways and peripheral blood [4], while long-term exposure is positively related to the mortality of cardiovascular disease and lung cancer [5–7]. The deposition of PM on the respiratory tract is mainly dependent on particle size [8]. It is found that smaller particles result in greater total lung and peripheral lung deposition as well as farther distal airway penetration [9]. Generally, particles with diameter larger than 10 μm can enter the nose and mouth. PM_{10} (subscript represents aerodynamic diameter no more than 10 μm) [10] can penetrate the trachea and bronchial regions, followed with the deposition at lung bifurcations [11]. Among them, particles larger than 8 μm tend to impact in the upper airways [12]. $PM_{2.5}$ and $PM_{0.1}$ can enter the non-ciliated alveolar regions, giving rise to deep deposition within the lung [11]. Since the particles smaller than 0.5 μm can be easily exhaled after penetrating the lung, $PM_{2.5}$ is considered to be a more serious threat to human health. Particles within this range can be stably deposited on respiratory tracts, easily access to cells, and transfer through blood and lymph circulations. The toxic PM can cause severe symptoms at some sensitive sites, e.g., bone marrow and heart [13]. Therefore, $PM_{2.5}$ is most widely employed to study the pathological, physiological and toxicological effects of PM on human health. PM is not only a fast-growing factor associated with early death but also impacts atmospheric conditions [14–16], and the accumulation of PM through years leads to climate change [17,18]. PM pollution is especially severe in developing countries due to economic growth and large populations. The average concentration of $PM_{2.5}$ in China in 2013 is 61 μg/m^3, while those in Europe and USA are 16 μg/m^3 and 10 μg/m^3 [19], respectively, nearly all exceeding the World health organization (WHO) guidelines (10 μg/m^3) [3].

It has been proved that upon inhalation of PM into alveoli, the particles initially interact with pulmonary surfactant, which maintains alveolar stability and modulates immune functions, impairing the phase behavior and metabolism of alveoli (Fig. 1). Meanwhile, adsorbate such as polycyclic aromatic hydrocarbons (PAHs), As and Pb may penetrate the surfactant to internal circulation and cause chronic and acute toxicities to human beings. Therefore, pulmonary surfactant is where the immediate health hazard occurs after PM enters respiratory tracts. There are many reviews summarizing the formation of PM and the possible hazards that PM brings about to human health [20–22], providing systematic introductions of how PM pollution affects the public and nature. Several reviews shed light on the interaction between nanoparticles and pulmonary surfactant [23,24] as well as the corresponding cellular and immune responses. However, most of the reviews were published nearly 10 years ago with many interaction mechanisms remained unclear. In recent years, several reviews have been published on the topic of particle-lung surfactant interactions [25–27]. The authors discussed the interactions of lung surfactant with inhaled nanoparticles or with particles that used in nanomedicine (especially drug delivery). Garcia-Mouton *et al.* emphasized the features of nanoparticles and the mutual effects of nanoparticles and surfactant [25]. Hidalgo *et al.* focused on the fate of the nanoparticles utilized as nanocarriers during their interaction with pulmonary surfactant, suggesting the application of surfactant in nanomedicine [26,27]. These reviews offer not only

summaries of particle-surfactant interactions, but also the implications for future nanomedicine.

In this review, summaries of composition and formation of both PM and pulmonary surfactant are first introduced. Then the interactions between various particles and pulmonary surfactants are discussed, followed by toxicological impacts of particles on lung surfactant, lung and other living cells and organisms. This review aims to highlight the recent progress on the *in vitro* research of the biophysical, physicochemical and morphological changes of pulmonary surfactant upon the exposure to PM, with a focus on the underlying intermolecular and interfacial interaction mechanism, correlating the fundamental investigations to surfactant functions and physiological performances of the lung and other tissues and organs. The particles investigated in the literature are mostly synthetic compounds and mixtures, while environmentally derived PM are also studied.

2. Composition and formation of PM

PM, a mixture of solids, liquids and gaseous matters in the air, commonly contains inorganic components such as sulfates, nitrates, ammoniums [28], crustal materials, sea salts [29], silicon, elemental carbon [30], and organic components such as organic carbon, quinones [31], polycyclic aromatic hydrocarbons (PAHs). Though organic compounds like quinones and PAHs are present with low amounts, their disease (e.g., cancer [32,33] and diabetes [34])-inducing effects cannot be neglected. The PM composition is complex and varies with time and locations. Usually, the chemical composition can be analyzed by inductively coupled plasma mass spectrometry [29], X-ray fluorescence spectrometry and ion chromatography [15]. Study of the composition enables us to figure out the sources and how PM affects public health and meteorological conditions.

There are two major sources of PM: anthropogenic activities and natural sources. Generally, naturally derived PM is from volcanoes, dust storms, living vegetation, etc., while anthropogenic PM is from fuel combustion, industrial and agricultural activities, traffic, etc. These sources lead to the spatial variation of PM composition and mass percent of each component. Mineral materials are the major contributor to PM composition as primary aerosol species, which is formed directly from source as particles (Fig. 2). The spatial variation of mineral materials in PM results from different crustal compositions. The PM dust collected in Northern China showed high levels of SiO_2 and CaO, along with low levels of K_2O and Na_2O, while some samples also contained heavy metals such as As and Pb. The main elements present in the dust including Si, Al, Fe and Ca are consistent with local crustal composition [35]. The mean concentration of mineral species in PM is usually higher in urban areas than that in other regions due to the influence of agricultural activities and unpaved roads. However, the rural areas in northwest China is an exception, where the low vegetation and forest cover results in a high level of mineral species in PM composition [28]. Another primary aerosol species-organic carbon was found of high levels in rural northwest China, urban South Asia, and High Asian Area (higher than 1680m a.s.l), where biomass burning is a determining factor. In contrast, the organic carbon levels in the USA and Europe are much lower [15]. The third largest primary aerosol species-elemental carbon is emitted with the highest levels in Asia and Africa [36] due to the incomplete combustion of carbonaceous materials [37]. NH_4^+, SO_4^{2-}, NO_3^- are three major secondary aerosol species that are formed during photochemical reactions in atmosphere. The urban to rural ratios of mass concentration of NH_4^+, SO_4^{2-} and NO_3^- during 2006 and 2007
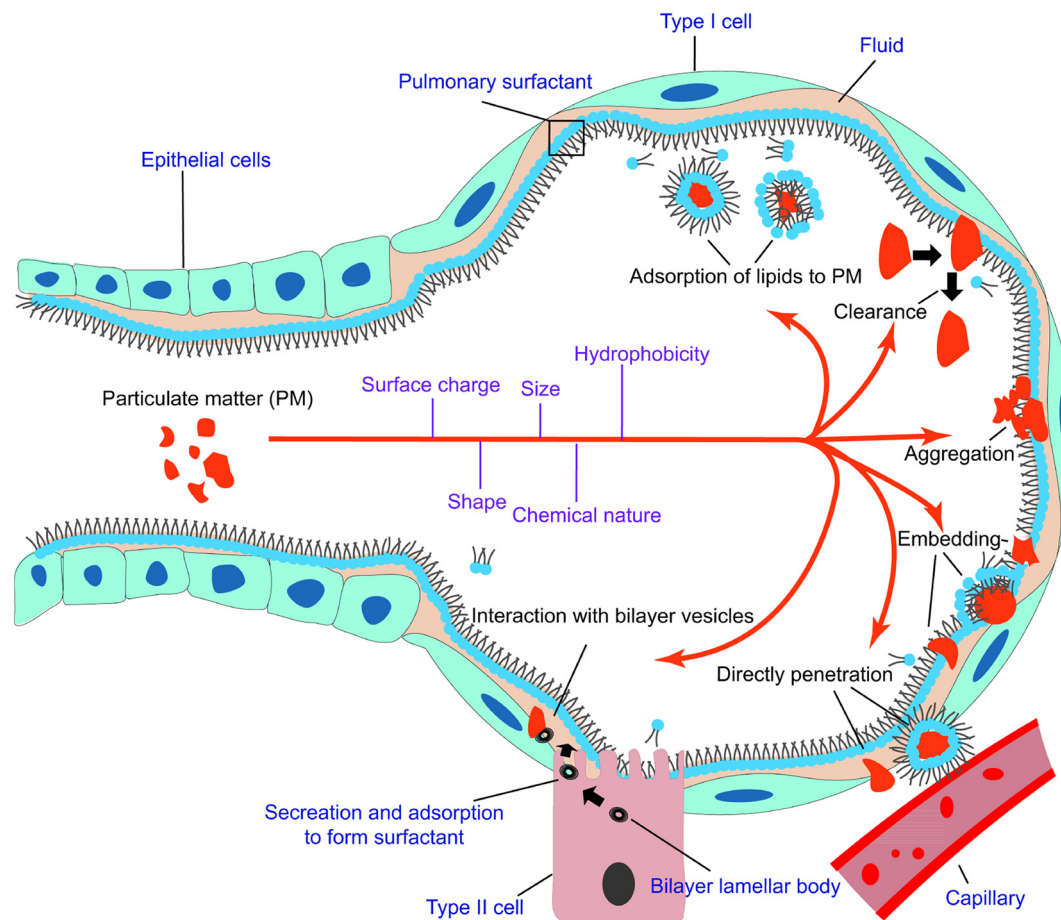
Fig. 1. Inhalation of PM into alveoli. The PM interacts with pulmonary surfactant in various ways depending on surface properties (surface charge, hydrophobicity, size, shape, etc.) of the particles. 1,2-dipalmitoyl-sn-glycero-3-phosphatidylcholine (DPPC) is used as the representative of lung surfactant. PM may embed into lung surfactant individually or in aggregates, with or without lipid wrapping. The defense mechanism of the surfactant can launch clearance to expel the impinging PM. PM can also penetrate lung surfactant to invade capillaries. The interaction of PM with bilayer vesicles would impede the metabolism of lung surfactant. Meanwhile, lipids may also transfer to the surface of PM to affect the behavior of PM in alveoli. This transfer also sequesters part of lung surfactant.

in China were 2.1, 2.2, and 1.9, respectively [15]. A similar trend was also observed in the Midwestern USA [28]. The relatively high concentration of SO_4^{2-} in urban areas is due to industrial and residential heating [38]. NO_3^- and NH_4^+ also mainly result from fossil fuel combustion [39], while the use of fertilizers and biomass burning contribute to NH_4^+ emission as well [40]. SO_4^{2-} was found with the highest emission in China, owing to economic growth and dense population which are in huge need of coal consumptions [15,41–43]. Unlike in China, the
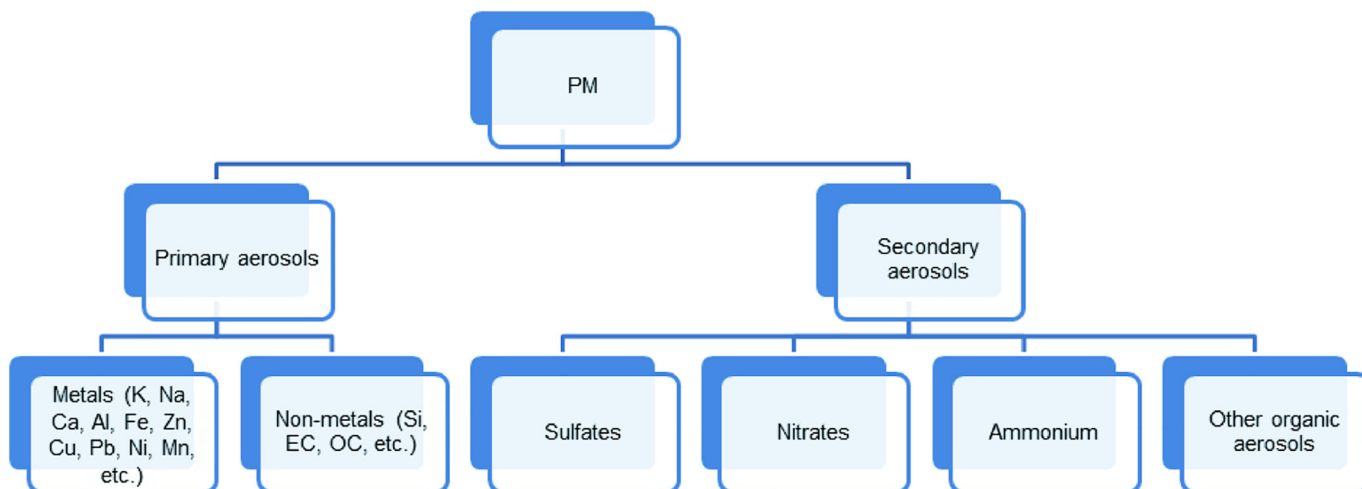
Fig. 2. Summary of the composition and sources of PM. OC: organic carbon; EC: elemental carbon.

elevated $PM_{2.5}$ concentration in the monitored sites in Iowa was mostly attributed to vehicular emission [28].

In addition to crustal composition and anthropogenic activities, terrain and meteorological conditions also play important roles in the discrepancy of PM composition among locations. Air stagnation is a meteorological phenomenon with features such as anti-cyclonic condition, high temperature, no precipitation and weak wind [44]. These features would result in the accumulation of PM pollution. High temperature accelerates the volatilization of ammonium nitrate. No precipitation means a lack of the scavenging sink to reduce $PM_{2.5}$. Air stagnation is strongly associated with terrain conditions. For example, the low elevation in eastern China, west coast in the USA and the Mediterranean basin gives rise to more frequent air stagnation, and thus PM pollutions in these areas are more severe than other surrounding regions. High altitude can also lead to air stagnation for peripheral areas where surface wind is blocked [19]. In addition to spatial variation, PM pollution exhibits a seasonal variation that can be ascribed to both anthropogenic activities and meteorological conditions [44,45]. In winters and springs, the air quality in China is always much worse, which is due to the heating that increases the secondary aerosol emission, and more stagnated air condition with a lower planetary boundary layer [17].

Along with the advent of nanotechnology, a myriad of nanoparticles have been produced in industry. These intentionally engineered nanoparticles become another source of PM pollution. Specifically, the application of inhaled targeted drug delivery in vaccines, therapeutics and diagnostics has provoked new concerns towards the potential adverse effects on human health [46,47].

3. Composition and function of pulmonary surfactant

Pulmonary surfactant is a mixture of surfactant proteins (SP-A, SP-B, SP-C, and SP-D) and lipids at alveolar air/liquid interface [48,49]. Pulmonary surfactant is a crucial part in physiological respiration [50]. It generally has three key functions: 1. preventing alveoli from collapse during respiratory activity, as it lowers the energy required for the alveoli to inflate by varying surface tension at the air/liquid interface; 2. defending against pathogen by killing them or preventing the dissemination; 3. modulating immune responses [51]. The first one is achieved through the film lipids enriched in dipalmitoyl phosphatidylcholine (DPPC). The viral defense and modulation of immune responses are mainly ascribed to the surfactant proteins (SP-A and SP-D).

Pulmonary surfactant contains four major surfactant proteins with critical functions, though their weight percentage (10%) is much lower compared with that of surfactant lipids (90%). Hydrophilic surfactant proteins SP-A and SP-D are Ca^{2+}-dependent lectins. Both SP-A and SP-D are involved in host-defense mechanisms and protection against viral infections [52,53] due to the structural similarities, e.g., C-terminal lectin domains which bind non-host oligosaccharides on viruses and bacteria [51]. Other structural characteristics contain NH_2-terminal domain, collagen-like region, and –COOH-containing carbohydrate recognition domain [54,55]. In contrast, hydrophobic surfactant proteins SP-B and SP-C are involved in the stabilization and formation of surfactant film. The detailed structural features and functions of the surfactant proteins are presented in Table 1.

Lipids comprise 90% of the mass of pulmonary surfactant. Phospholipids contribute 80%~90% to the mass of lipids while cholesterol, triglycerides, and fatty acids occupy the remainder. Phosphatidylcholine (PC) is the most abundant phospholipid (80~85% of phospholipids) in pulmonary surfactant, with disaturated compound dipalmitoyl phosphatidylcholine (DPPC) as the major component of PC. Other phospholipids include phosphatidylglycerol (PG), phosphatidylinositol (PI), phosphatidylethanolamine (PE), and phosphatidylserine (PS). PG is the second abundant phospholipids (7~15% of phospholipids) while PI, PE, and PS occupy less than 5% for each [51,68]. The structures and functions of some representative lipids are illustrated in Table 2.

Table 1
Summary of surfactant proteins.

Proteins	Structural features	Examples of Functions
SP-A (i) [a]	Octadecameric glycoprotein, 650 kDa [56], acidic	Facilitates clearance of pathogens and immune effectors [57], inhibits secreted phospholipases A_2 activity and maintains surfactant integrity during lung injury [58]
SP-B (o) [a]	79-amino-acid homodimer with disulfide-linked, 18 kDa [59]	Enhances adsorption of phospholipids from subphase to interface [60]. Increases collapse pressure of fatty acids to avoid "squeeze-out"
SP-C (o) [a]	Nonpolar α-helical protein containing 35 amino acids, 4.2 kDa [61]	Stabilizes phospholipids [62,63], increases viscosity of interfacial film [64]
SP-D (i) [a]	Glycoprotein, dodecamer of four trimmers, 43 kDa [65]	Regulates surfactant metabolism [66], promotes epithelial cells to uptake pathogenic bacteria [67]

[a] "i" represents hydrophilic and "o"represents hydrophobic

Surfactant proteins play important roles in film stabilization and viral defense, while surfactant lipids are ultimately responsible for surface tension change during respiration [69]. DPPC, the major component that occupies 30–45% of pulmonary surfactant [86], is a zwitterionic molecule that contains two hydrocarbon tails and a polar head. The gel-to-liquid crystal melting transition of DPPC occurs at 41°C, which makes DPPC a condensed phase at physiological temperature [69]. The condensed phase of DPPC endows it an ability to reduce surface tension to near zero at the end of exhalation. This property results from the highly packed alignment of DPPC molecules at air/liquid interface [48,87]. When alveolus is inflated or deflated, the surface pressure difference required (ΔP) is proportional to surface tension (γ) divided by the radius of the alveolus (R), which can be described by Laplace equation (1).

$$\Delta P = 2\gamma/R \tag{1}$$

If the surface tension of alveolus remains high during exhalation, the pressure difference would increase with decreasing radius, making the pressure in the smaller alveolus higher than that in the larger alveolus. Because of the interconnected structure of alveoli, the smaller ones would collapse to larger ones [88,89]. The presence of DPPC in lung surfactant can effectively solve this problem by reducing the surface tension.
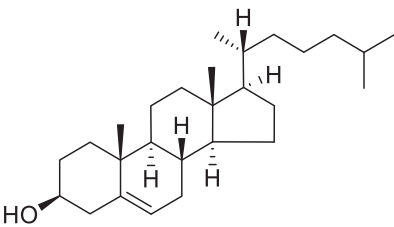
The pulmonary surfactant can stabilize the alveoli during respiration via two processes. First, after the secretion of bilayer vesicles in alveolar subphase, lipids, proteins, and other components are adsorbed quickly onto the air/water interface to form an interfacial film. During the adsorption process, SP-B and SP-C lower the energy barrier for this energetically-unfavorable transfer and stabilize the intermediates involved, ensuring this process is fast enough on the scale of seconds [90]. Second, when the surfactant film is compressed by the shrink of alveolus and the surface pressure is elevated, the film would stay at the interface to reduce the surface tension to minimize the volume change of alveoli. Until the maximum surface pressure (Π_e) is reached, the film transits from a two-dimensional structure to a three-dimensional structure and the collapse of film occurs [69]. The alveolar collapse would be avoided in lung due to the surfactant. When the film containing disaturated phospholipids (e.g., DPPC) and unsaturated lipids (e.g., POPC and POPG) is transferred to the air/liquid interface and compressed, liquid condensed (LC) domains with ordered packing and quasi-crystalline organization are formed and floating in a much more disordered phase called liquid expanded (LE) phase. If cholesterol is present in the film, it would modulate the organization and dynamics of the phases, converting the LC/LE coexistence to liquid ordered/liquid disordered coexistence [90]. A classical model indicated that the

Table 2
Summary of Surfactant Lipids

Components	Structures	Properties and Functions
1,2-dipalmitoyl-sn-glycero-3-phosphatidylcholine (DPPC) (PC16:0/16:0)		Remains as a condensed phase at physiological temperature [69]. Generates a near-zero surface tension [70].
1-palmitoyl-2-oleoyl-sn-glycero-3-phosphocholine (POPC) (PC16:0/18:1)		Melting point -3°C [71]. Makes the membrane fluid at physiological temperature [72].
1-Palmitoyl-2-palmitoleoyl-sn-glycero-3-phosphocholine (PPPC)(PC16:0/16:1)		Related to surface dynamics of surfactant [73] and respiratory rate [74].
1-palmitoyl-2-myristoyl-sn-glycero-3-phosphocholine (PC16:0/14:0)		Modulates macrophage that related to alveolar protection [75]. Related to respiratory rate [74]
1,2-dipalmitoyl- sn-glycero-3-phosphoglycerol (DPPG)		Reduces permeability of benzo[a]pyrene [76]
1-palmitoyl-2-oleoyl-sn-glycero-3-phosphoglycerol (POPG)		The most prevalent PG in human surfactant. Inhibits macrophage proinflammatory and TLR2-dependent inflammatory responses [77], has an antivirus function [78], makes the film more fluidized [79].
Phosphatidylserine (PS)[a]	e.g.	Determines the cellular and subcellular distribution of quinidine [80]. Regulates the activities of several enzymes in cell signaling [81]
Phosphatidylethanolamine (PE)[a]	e.g.	Causes lateral pressure and introduces curvature stress to stabilize membrane proteins [82,83]
Phosphatidylinositol (PI)[a]	e.g.	Increases the rate of alveolar fluid clearance [84]. Involved in the stabilization of surfactant monolayer [81]

Table 2 (continued)

Components	Structures	Properties and Functions
Cholesterol		Increases the fluidity of surfactant [85]

^a Only one representative structure of each minor phospholipids PS, PE, and PI is illustrated.

interfacial film only contains a rigid condensed phase during compression, which implies the retainment of DPPC in the film and "squeezed out" of all other components, especially fluid lipids, to the subphase to promote low surface tension [91]. The "squeezed out" part remains underneath as a reservoir for the expansion. The reservoirs underneath are multilayered and multilamellar structures interconnected with the interfacial monolayer film by surfactant proteins, which facilitates the fast diffusion of surface active species to the interface upon expansion [92]. However, many pieces of evidence proved that the film under compression is not that condensed, suggesting a coexistence of LC, LE and collapsed phases [93,94]. An observation further revealed that the concentration of DPPC at the interfacial film was reduced during compression, which implies that in addition to fluidizing lipids, some DPPC may also be squeezed out [95]. The synergistic effect of surfactant proteins and lipids keeps the alveolar lining in a metastable status, preventing lung collapse during respiration.

4. Interactions of particulate matter and pulmonary surfactant

A variety of nanoparticles, such as simple metal oxides [96–100], non-metal oxides [101,102], polymer-coated and polymer nanoparticles [103–105], metal nanoparticles [106–108], carbon nanomaterials [100,109], and other compounds containing carcinogenic matters [110–113], have been investigated in the studies of particle-surfactant interactions. A few studies on environmental PM dust exposure have also been conducted [110,114,115], but they are still in the very early stage compared to those using engineered nanoparticles. One challenge is the variety of composition, size, and other biological and physical properties of $PM_{2.5}$ due to geographic locations and seasons. This variety also contributes to the high heterogeneity and complicity of the particles, which creates difficulties in identifying and characterizing the effect of each component. Many engineered nanoparticles such as silica and aluminum oxide are also present in PM dust, therefore in many studies, engineered nanoparticles are used as substitutes of environmental PM to provide implications for air pollution.

DPPC is a commonly used surfactant model because of its dominating proportion in natural pulmonary surfactant and the convenience of preparation and characterization. Some natural lung surfactants derived from mammals are also used in the light of physiological relevance. These natural surfactants are comprised of not only DPPC but also surfactant proteins and other lipids that may exist in human lungs. In most studies, surfactant molecules are dispersed as monolayers or bilayers to explore the interaction with particles. Langmuir monolayer has been widely utilized because it is an essential surfactant model of biological relevance [116,117]. The studies of bilayer and multilayer structures which are more physiological relevant have also been conducted using newer characterization methods.

PM adheres to pulmonary surfactant by various types of interactions, such as electrostatic forces, hydrophobic interactions, van der Waals forces, etc. Among them, electrostatic forces and hydrophobic interaction primarily depend on the surface charge and surface hydrophobicity of PM, respectively, while van der Waals force is ubiquitously distance-dependent which arises from the inherent movement of electrons. The interaction potential (energy), w(r), and force, F(r) of van der Waals interaction between two atoms or small molecules can be obtained as follows:

$$w(r) = -C_{vdW}/r^6 \qquad (2)$$

$$F(r) = -6C_{vdW}/r^7 \qquad (3)$$

Here, r is the interatomic distance, C_{vdW} is the interaction constant which is given by

$$C_{vdW} = -\left[\frac{\mu_1^2\mu_2^2}{3(4\pi\varepsilon_0\varepsilon)^2 k_B T} + \frac{\mu_1^2\alpha_2 + \mu_2^2\alpha_1}{(4\pi\varepsilon_0\varepsilon)^2}\right]_{v=0}$$
$$+ \left[\frac{3\alpha_2\alpha_1}{2(4\pi\varepsilon_0\varepsilon)^2}\frac{h\nu_1\nu_2}{\nu_1 + \nu_2}\right]_{v>0} \qquad (4)$$

where μ_1 and μ_2 are the dipole moments, α_1 and α_2 are the electronic polarizabilities, ε_0 is the vacuum permittivity, ε is the relative dielectric constant of the surrounding medium, k_B is the Boltzmann constant, T is the temperature, ν_1 and ν_2 are ionization frequencies, h is the Plank constant [118]. Equations (2) and (3) express the van der Waals interactions at the atomic level, which can be applied to the interactions between the component molecules of PM and lung surfactant molecules. Equations (5)–(8) supplement the theories of van der Waals interactions at larger scales, e.g., surface level, for cases surfactant films interacting with component molecules of PM (Eq. 5, 6) or with the whole PM particles (Eq. 7, 8)

$$w(d) = -\frac{\pi C\rho}{6d^3} \qquad (5)$$

$$F(d) = -\frac{3\pi C\rho}{6d^4} \qquad (6)$$

$$w(d) = -\frac{AR}{6d} \qquad (7)$$

$$F(d) = -\frac{AR}{6d^2} \qquad (8)$$

where d is the distance between the interacting objects, C is the interaction constant that is decided by the molecule's property, ρ is the number density of molecules of the surface material, A is the Hamaker constant [119], R is the radius of the sphere. Equations (5) and (6) illustrate the van der Waals interaction energy w(d) and the force F(d) between atoms and surfaces, while equations (7) and (8) describe that of sphere-flat surface systems. Equations (2)–(8) are applied to the circumstances where the interaction range and separation are much

smaller than the radii of the interacting objects. It is obvious that van der Waals force is greatly dependent on the distance between the surfactant and PM. Equations (2)–(8) can be used to estimate the interactions for neutral PM-surfactant systems, or to evaluate the van der Waals force for charged PM-surfactant systems where van der Waals force contributes to the net interfacial interaction.

PM impacts pulmonary surfactant in many aspects, including phase behavior, stability, compositions, morphology, etc. Particles may be retained in surfactant forming aggregate domains, or surfactant may be adsorbed to the surface of particles, thus the concentration, elasticity, lateral diffusional property, compressibility, and adsorption behavior of the surfactant are changed, which directly affects the biophysiological properties of surfactant. Particles may also penetrate through surfactant linings to induce inflammation, oxidative stress, or other cytotoxicity and genotoxicity to surfactant and epithelial cells, which is considered an indirect effect on alveolar lining. The transport of particles in monolayers is determined by the Brownian motion and the drag force exerted on the particles from the film. The mean-squared displacement of Brownian motion is

$$\langle x^2 \rangle = 6Dt \text{ or } 4Dt \tag{9}$$

where 4Dt is for the particles that are attached to the film to undergo two-dimensional lateral movement. D is the diffusion coefficient and t is the lag time [120]. The viscosity of the surfactant film influences the diffusion according to Stokes-Einstein equation

$$D = k_B T / 6\pi\eta R \tag{10}$$

where k_B is the Boltzmann's constant, T is the temperature, η is the viscosity of the film, R is the radius of particle. Because of the high viscosity of the surfactant, additional drag force causes a decrease in diffusion coefficient. Drag coefficient ζ is expressed in equation (11)

$$\zeta = k_B T / D \tag{11}$$

where k_B is the Boltzmann's constant, T is the temperature, D is the diffusion coefficient. For larger particles (i.e., particles with diameter larger than 200 nm), the drag exerted due to the high viscosity of the surfactant is added to the Einstein-Stokes model, leading to Danov−Aust−Durst−Lange (DADL) model [121,122] where the diffusion coefficients are given by

$$D = \frac{k_B T}{6\pi\eta R + \sigma R^{0.1}} \tag{12}$$

$$\sigma = 8\pi\eta \left(0.22 \left(\frac{2\eta}{\eta_m} \right)^{-0.9} \right) \tag{13}$$

where η_m is the two-dimensional viscosity. Equations (9)–(13) prove that the translocation of PM within the surfactant is affected by the viscosity of the surfactant and temperature.

4.1. Instrument, methodologies and characterization

4.1.1. Langmuir-blodgett trough and surface pressure – area isotherm

The instrument that is prevalently utilized in the research of interactions between pulmonary surfactant monolayers and nanoparticles is Langmuir-Blodgett trough (LB trough) (Fig. 3A). The trough can be used to prepare thin molecular films at air/liquid interface. The back and forth of two opposite barriers change the surface area of the film through compression and expansion, which simulates the status of pulmonary surfactant during respiration [123]. During the expansion and compression, surface tension of the film is continuously measured with a Wilhelmy plate (balance), and a plot of molecular area versus surface pressure is then generated. This surface pressure - area (Π - A) isotherm clearly depicts the phase behavior of the interfacial
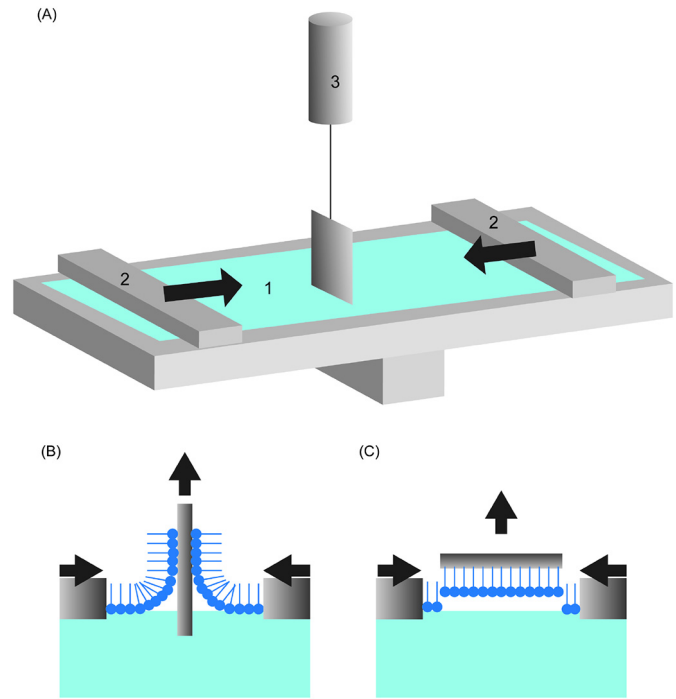
Fig. 3. (A) Schematic of Langmuir-Blodget trough with Wilhelmy balance. 1: air/liquid interface covered by molecular film, 2: movable barriers that can proceed to expand and extrude the film, 3: pressure sensor with Wilhelmy plate. A surface pressure- molecular area (Π – A) isotherm can be obtained with the read-out of Wilhemy plate and barriers (B) Schematic of Langmuir–Blodgett technique (vertical deposition). (C) Schematic of Langmuir–Schaefer technique (horizontal deposition)

film. Technically, LB trough is applicable to amphiphilic molecules that can form stable Langmuir films on air/liquid interface. Besides a tool for interfacial property study, LB trough can also be used to fabricate highly organized multilayer structures. Langmuir films can be transferred to a substrate by either Langmuir-Blodgett (LB) technique that utilizes vertical lifting (Fig. 3B), or Langmuir-Schaefer (LS) technique with horizontal lifting (Fig. 3C). Multiple layers can be obtained with LB technique by repeating dipping and lifting cycles [124]. LB technique always leads to low surface coverage for non-amphiphilic molecules because of aggregation. LS technique gives rise to a uniform film of high quality on substrate [125], though a multilayer film cannot be obtained.

There are several different methods to expose lung surfactants to PM. One is to mix the surfactant solution with particles and then inject the mixture onto the interface by microsyringe [101,103,108,112,126]. This conventional method enables an easier control over the feed ratio, and a sufficient exposure of surfactant to particles can also be achieved. Nevertheless, the observation of the adsorption behavior of particles to surfactant is ruled out since the mixing results in some adsorption before measurement. The manual mixing disqualifies this exposure method to simulate the natural inhalation process. Another method is dispersing particles in a subphase and a lipid solution is spread on the interface either after [96,98,109,127–129] or before particle dispersion [99], as in the latter situation the particle solution is injected through the lipid film to the subphase. This method is adequate to study adsorption behavior but requires a large number of particles, and the diffusion of colloidal particles in subphase would greatly affect the adsorption process. Besides the above mentioned strategies, it is also possible to deposit surfactant to air/water interface, and then colloidal particles are spread on the interface from air side [110,130]. This process is more similar to the natural exposure process of lung lining to PM than the previous ones. A dry powder insufflator has been used to generate and apply particle aerosols to surfactant, which mimics how lung surfactant is actually exposed to PM. In the study conducted
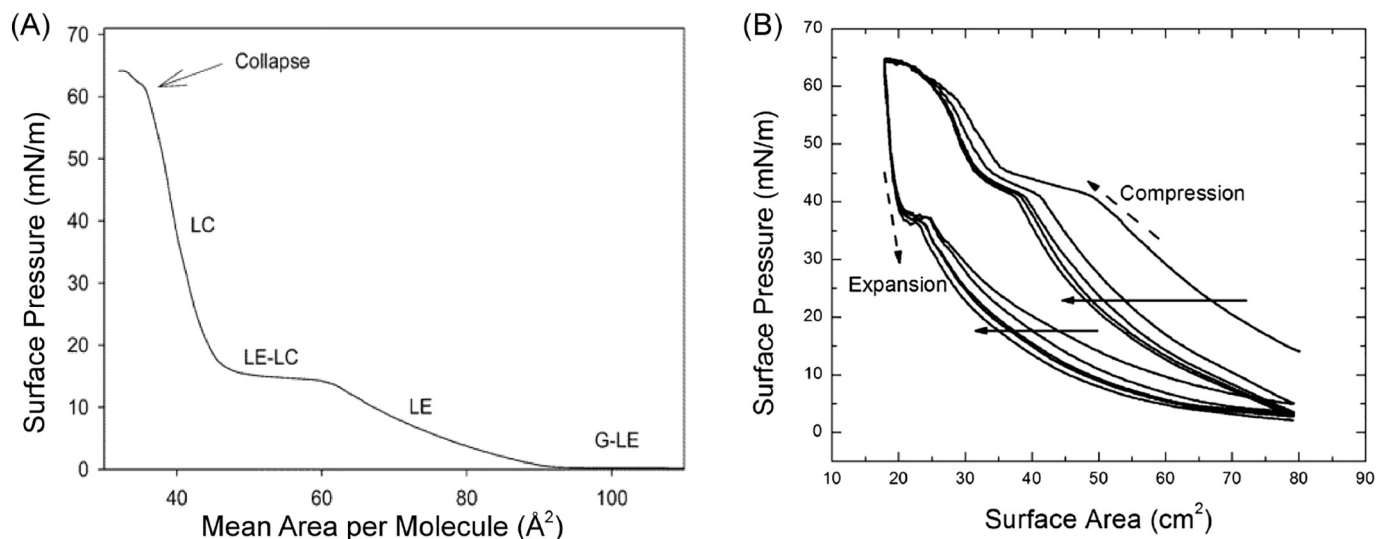
Fig. 4. (A) Surface pressure versus surface molecular area (Π – A) isotherm of deuterated DPPC-d$_{62}$, LC: liquid condensed, LE: liquid expanded, LE-LC: coexistence of LE and LC phases, G: gas phase, G-LE: coexistence of gas and LE phases. Temperature: 24°C. Subphase: pure water. [132]. Adapted with permission from Ma *et al.* [132]. Copyright (2006) American Chemical Society. (B) Π - A Isotherm of pure lung surfactant over five compression and expansion cycles. This isotherm is presented in terms of the trough area. The solid arrows indicate the progression from the first cycle to the fifth. The dashed arrows show the directions of compression and expansion. Only "squeeze-out" plateaus around 42 mN/m representing transition from monolayer to multilayer are observed during compression. The change in slope can tell the phase transition. The expansion curves exhibit elastic stretching around 37 mN/m. [130]. Adapted with permission from Kodama *et al.* [130]. Copyright © 2014 Biophysical Society. Published by Elsevier Inc.

by Farnoud *et al.* [131], aerosols were applied to surfactant during the whole compression process instead of solely at 0 mN/m. This operation implies the importance of particle deposition on compressed films in the study of particle-surfactant interaction.

The phase behavior of the surfactant films on air/liquid interface can be evaluated based on isotherms of molecular surface area versus surface pressure. An isotherm example of pure deuterated DPPC-d$_{62}$ shows obvious LE-LC transition and coexistence (Fig. 4A). The transition plateau of gas to LE indicates that DPPC starts to be compressed to a two-dimensional liquid. With further compression from LE to LC, DPPC transits from a liquid to a two-dimensional packed semicrystalline phase. In the LC phase, the tails of DPPC molecules are aligned and pointing out to the air, while water molecules are squeezed out, leading to a dehydrated, poor re-spreading DPPC film with poor adsorption ability [132]. Finally, DPPC collapses at maximum surface pressure (π_e). In contrast, the LE-LC coexistence plateau is not shown for natural surfactant due to the multicomponent. For example, in Fig. 4B, the transition of LE to LC-LE coexistence exhibits as a change in the slope around 15 mN/m.

LB trough can also be used to monitor the surface pressure change of lung surfactant during dynamic compression-expansion cycles, giving rise to a better understanding of its surface activity under breathing conditions. Fig. 4B shows typical surface pressure change of Survanta during compression-expansion cycles which can mimic the expiration-inspiration process. Following the collapse during compression, the film was immediately returned to the fully expanded area, with an elastic stretch occurring at the drastic decrease of surface pressure. This stretch was due to the recovery of the film from folds and collapse. During compression, the flat around 42 mN/m is a "squeeze out" plateau, where the unsaturated lipids that cannot stand high pressure are squeezed out to the subphase as a reservoir. Saturated lipids and fatty acids are left to form a condensed phase. Upon expansion, part of the reservoir is re-adsorbed to the interfacial film while the rest materials are permanently lost. This phenomenon is exhibited as a hysteresis loop between the compression and expansion curves (Fig. 4B) [133,134]. The hysteresis area can be used to indicate the stability and respreadability of the surfactant film, where a larger loop represents a higher degree of inhibition caused on the surfactant. Due to the

expelling of partial surfactant at the end of the first collapse, the second compression curve significantly shift to a smaller surface area compared with the initial one. Similar shifts also occur for the following consecutive cycles.

The surface pressure of the monolayers is affected by temperature, molecular area, the numbers of ions, etc. Because of different contributions of LE and LC phases to surface pressure, there are two separate Eq. (14) and (15) which are in a good agreement with experimental Π-A curves [135]:

$$\Pi = \frac{mkT}{A_0 - \omega} - \Pi_{coh} \tag{14}$$

$$\Pi = \frac{mkT\alpha\beta}{A_0 - \omega[1 + \theta(\alpha\beta - 1)]} - \Pi_{coh} \tag{15}$$

Eq. (14) is for LE state and Eq. (15) is for the coexistence state of LE and LC. In these two equations, m is the number of kinetically independent units per monolayer molecule, k is the Boltzmann's constant, T is the temperature, A_0 is the actual area required for each lipid molecule, ω is the particle molecular area, Π_{coh} is the cohesion pressure that accounts for the intermolecular interaction, θ is a coefficient related to the area per mole of monomer in a cluster, α and β are expressed as follows:

$$\alpha = \frac{A_0}{A_c} \exp\left[-\theta \frac{\Pi - \Pi_c}{kT}\omega\right] \tag{16}$$

$$\beta = 1 + \frac{\omega(1 - \theta)(\alpha - 1)}{A_0} \tag{17}$$

where A_c is the molecular area that corresponds to the area at the onset of transition, Π_c is the surface pressure of the transition commencement [135,136]. It is noted that the predictions in Eq. (14) and (15) are unrestrictedly convincing only within low-pressure range.

Besides phase transition behavior, compressibility, elasticity, viscosity, etc. can also be derived from Π-A isotherms. The compressibility C_s is expressed as equation (18)
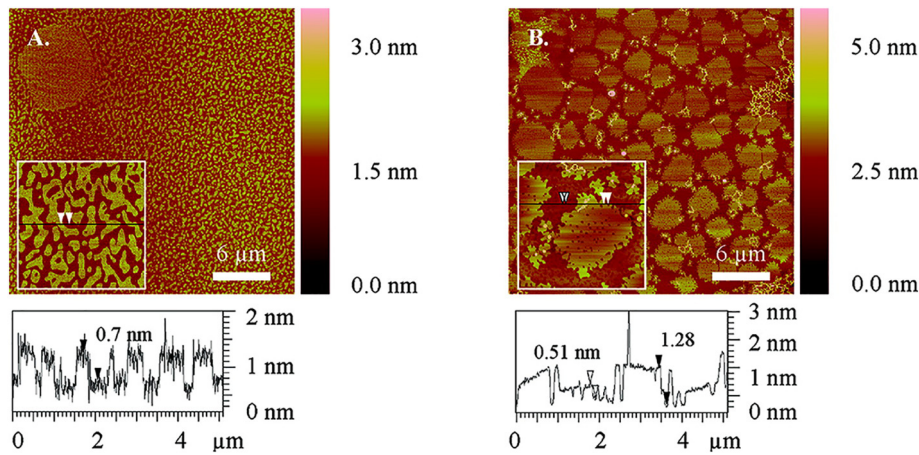
Fig. 5. AFM images of mica-supported pure DPPC monolayer (A) and 99.8 mol% DPPC + 0.2 mol% hexadecanethiolate-capped Au NPs (C$_{16}$SAu NPs) (B) at 3mN/m. These monolayers were obtained by Langmuir-Schaefer (LS) deposition technique. Light color represents larger height levels while dark color represents low height levels. The height profiles under the images exhibit different phases displayed in the monolayers. The arrows in the height profiles correspond to those in the insets. In pure DPPC monolayer, large circular LC domain with LE-lipid-filled hole defects (top left in A), small micro LC domains (inset in A) and continuous LE phase are present. In NP-containing monolayer, in addition to LE and LC domains, there are also pinhole defects (darkest color) in both domains (insets in B) and stringe-like C$_{16}$SAu NPs aggregates (lightest color). The sizes of the main images are 30 μm × 30 μm and those of the insets are 5 μm × 5 μm. [108]. Reprinted with permission from Tatur *et al.* [108]. Copyright (2012) American Chemical Society.

$$Cs = -\frac{1}{A}\left(\frac{\partial A}{\partial \pi}\right) \tag{18}$$

where A is the molecular area and Π is the surface pressure. Elasticity is the reciprocal of compressibility. The higher compressibility (lower elasticity) represents a more diluted monolayer with weak intermolecular interaction. Low compressibility is beneficial for surfactant function because it enables surfactant films to reach zero surface tension rapidly with a small change of surface area.

In addition to LB trough, pulsating bubble surfactometer [137], captive bubble tensiometer [138] have also been used to measure the surface activity of lung surfactant.

4.1.2. Atomic force microscopy and domain images

The morphological properties of pulmonary surfactant are studied by atomic force microscopy (AFM) [139] after a Langmuir film is transferred onto a substrate or by Brewster angle microscopy (BAM) directly on air/liquid interface. In AFM images, pure DPPC exhibits regular patterns where the dark LE phase is distinguished from the bright LC phase (Fig. 5). The shapes and sizes of the domains change with the extent of compression. The shapes are determined by two competing forces: one is the long-range dipole-dipole repulsion which leads to an elongated domain, and the other is the boundary tension (γ) that forces a domain to exhibit a circular shape to minimize the tension [140]. The optimal diameter of LC domain is determined by equation (19)

$$D_0 = \frac{e^3\delta}{2} exp\left[\frac{4\pi\varepsilon\varepsilon_0\gamma}{(\Delta m)^2}\right] \tag{19}$$

where e is the natural constant, δ is the molecular dipole distance, ε is the dielectric constant of water, ε_0 is the dielectric constant of vacuum, Δm is the dipole density difference between phases [141–144]. The disconnected LC domains move by Brownian motion, repelled by each other and the LE domains to avoid coalescing. The previous studies showed that the introduction of particles to the surfactant leads to changes in domain shape and size. For example, alkylated Au nanoparticles (NPs) disrupt the network of microdomains and cause pinhole defects in both LE and LC domains (Fig. 5).

The fractions of LC and LE domains determine the viscosity of lung surfactant, thus the translocation of particles in the surfactant is affected. The overall viscosity of the film (η_s) is denoted in equation (20)

$$\eta_s/\eta_{so} = (1-A/Ac)^{-1} \tag{20}$$

where η_{so} is the shear viscosity of the continuous LE phase, A is the area fraction of LC and Ac is the critical LC fraction where the LC domains start to merge and the viscosity diverges [145]. As a result, the translocation of particles within lung surfactant is greatly influenced by the compression extent of the film [146]. In addition to AFM, other instrument such as fluorescence microscope [147] can also be used to study the morphological change of lung surfactant when interacting with PM.

4.1.3. Surface Forces Apparatus (SFA)

Surface forces apparatus (SFA) is similar in some ways to AFM that generally measures the force between a sharp tip and a surface, which detects the force between two curved surfaces. In these techniques, both the tip and the surfaces can be functionalized with desired molecules [148]. SFA has a unique feature of measuring the interaction forces as a function of the absolute separation between two surfaces, which is especially useful for soft materials [149,150]. The interfacial force is measured based on the Hooke's Law by detecting the deflection of the double cantilever spring [151], while the surface separation distance is monitored in real time using an optical technique called multiple beam interferometry [152]. Lung surfactant lipids can be deposited onto substrate surfaces (e.g., mica) as monolayers, bilayers or multilayers by LB trough and then be applied for force measurements in aqueous media using SFA. The surface force measurements can provide useful information regarding the particle-lipids systems. Moreover, the measurement of interfacial forces within surfactant lipids monolayers and bilayer systems can offer important information and interactive monitoring of the membrane fusion during PM-deposition.

SFA have been widely applied for quantifying a variety of forces in both biological [148] and non-biological systems [153], such as van der Waals forces, electrical double forces, hydrophobic interaction [154] and solvation forces (e.g., hydration interaction). The interfacial forces between different surfactant components have been directly quantified using an SFA [155]. In this study, the stability of the bilayers during surface interaction was evaluated by detecting the occurrence of hemifusion using SFA. Lee *et al.* [156] obtained real-time images of domain reorganization and force-distance profiles of lipid bilayers during membrane hemifusion using a fluorescence SFA. They demonstrated that the domains tend to rearrange in order to decrease the energy barrier and increase the fusion rate in the membranes. This technique

correlates fluorescence imaging with force measurements, which is applicable to monitor dynamic rearrangement and adsorption processes in lung surfactant monolayers and bilayers.

4.1.4. X-Ray scattering and Other Techniques

The structural information of lung surfactant at air/water interface can be obtained with several techniques, such as x-ray scattering, neutron reflectivity and sum frequency spectroscopy. X-ray scattering is a family of sensitive and nondestructive analytical techniques to characterize the chemical composition, crystal structures and physical properties of thin films and other materials. These techniques can be used to investigate biological membranes directly and *in situ* at the air/water interface under near physiological conditions [157]. The techniques of x-ray scattering include x-ray reflectivity (XR), grazing incidence X-ray diffraction (GIXD), x-ray diffraction, etc. In XR, x-rays are reflected from a flat surface and measured. XR is useful to measure layer thickness of thin films and multilayers, surface density gradients and layer density, and surface roughness. This technique can easily distinguish monolayer from bilayers or multilayers [158] due to the reflectometry pattern produced from the interference of the reflected beams from each interface. Usually, a surface normal electron density profile is acquired in XR. The in-depth structural change of surfactant monolayer can be revealed from the visible interference fringes and distinct features in XR curves [159]. In addition to the outer part of monolayer structures, XR is also very sensitive to layered lung surfactant due to the presence of ionic lipids with high density of electrons in the headgroups [158]. GIXD provides information about atomic order, crystallinity and molecular orientation of surface and layers. GIXD is generally used in combination with XR, which gives a more comprehensive picture of three-dimensional distribution of lung surfactant [127,160].

Neutron reflectivity is similar to x-ray reflectivity, where a beam of neutrons is shined onto a flat surface and then reflected and measured. The magnitude of neutrons irradiation can be very high, for example, for hydrogen and deuterium, which leads to high contrast in the measurement. Neutron reflectometry has been widely used to observe the structures of bilayers attaching to monolayers or more bilayers at the air/water interface [161]. The multilayers of bovine- and porcine-derived pulmonary surfactant at the air/water interface were investigated by neutron reflection, showing a disordered lateral surface with lipid/protein bilayers alternating with aqueous layers [162]. The repetition period and correlation depths were also measured to be 70 Å and 3 to > 25 bilayers, respectively.

Sum frequency generation vibrational (SFG) spectroscopy is a second-order nonlinear optical technique. This coherent vibrational spectroscopy possesses selectivity of infrared and Raman spectroscopies together with surface sensitivity. It is a potent tool to study the structure and orientation of different biomolecules such as lipids since the vibrational spectra detected are determined by fundamental molecular structure. For example, in the investigation of the interaction between DPPG bilayers and melittin, the C-H and C-D stretching signals were measured from isotopically symmetric and asymmetric DPPG bilayers, providing real-time information of the structural perturbation, such as water alignment and adsorption kinetics, on the bilayers [163].

4.2. Studies of PM with different surfactant systems

DPPC is the most common lipid in biological membranes (e.g., pulmonary alveoli lining) and DPPC monolayer has already been well-characterized by many researchers [164]. Therefore, DPPC monolayer is widely used as a simple model of lung surfactant in particle-surfactant studies. In addition, investigations on DPPC monolayer can lay the foundation for studies on other complex biological membrane systems. Hao *et al.* [99] measured the adsorption behavior of Fe_3O_4 to DPPC monolayers. With the introduction of Fe_3O_4, the isotherm of DPPC shifted to larger surface areas and the extent became larger with increasing concentration of nanoparticles. This observation implies

that the nanoparticles were adsorbed into the monolayer. Generally, the isotherm shifts observed in most studies are similar because the nanoparticles investigated are always much larger than DPPC or other lipid molecules. The isotherms shift to larger molecular areas to account for the areas occupied by the introduced particles [165]. The AFM images of DPPC with Fe_3O_4 showed that the nanoparticles formed granule domains on the monolayer, reducing the elasticity of the monolayer. This interaction was considered as the electrostatic attraction between the negatively charged phosphate and positively charged Fe_3O_4 particles.

Clinical lung surfactant has been used to compare with pure DPPC monolayer. Infasurf is a clinical lung surfactant extracted from calf lung fluid. The composition is more complex and closer to human lung surfactant than pure DPPC. In the research conducted by Farnoud *et al.* [131], the Π-A isotherms of DPPC and Infasurf monolayers only showed slight changes upon the deposition of carboxylated modified polystyrene nanoparticles. Nevertheless, the maximum surface pressure of the DPPC monolayer kept decreasing with every compression and expansion cycle, due to the loss of DPPC from the air/water interface at the end of each cycle. Upon collapse, nucleation occurs at the phase boundary due to the curvature because the film cannot be compressed further without destabilization. The decrease in the energetic barrier for nucleation leads to the formation of bilayer folds and other two-to-three-dimensional transformation, especially when there are plenty of nuclei [166,167]. The presence of the carboxylated modified polystyrene could provide nucleation sites and reduce the pressure required for collapse, facilitating the collapse of the film during compression [168]. This inhibitory effect was diminished on Infasurf, and the phase behavior was restored after five cycles. This result suggests that *in vivo*, the particles investigated may not inhibit the function of lung surfactant. Moreover, the reduction of the maximum surface pressure of Infasurf was less than that of DPPC, indicating that less Infasurf was squeezed out, or the replenishment of Infasurf was faster than pure DPPC [131]. This phenomenon is consistent with the functions of the SP-B and SP-C present in Infasurf. Other commercial pulmonary surfactants such as Survanta [108,130,169], Curosurf [98,101,104] are also used to test how exogenous PM affects their phase behavior and morphology. Survanta is a natural bovine lung extract that contains a large fraction of fatty acids and triglycerides (10% ~20% with respect to DPPC by weight) but does not contain SP-A [133]. Curosurf is extracted from porcine lung surfactant, and 99% of the contents are lipids, with 1% SP-B and SP-C. The investigation of pure DPPC and Survanta conducted with alkylated Au NPs indicates that the domain formation in both systems was affected by the presence of NPs. In DPPC, the LE phase formation was promoted while the LC phase formation was hindered [108]. In Survanta, the SP-B and SP-C induced the formation of many small condensed domains [170]. The alkylated Au NPs accumulated in the LE phase in Survanta and merged into the hydrophobic proteins [108]. The presence of surfactant proteins also results in a higher foaming ability, which is an essential property for the surfactant to maintain interfacial property [111]. The foaming ability would be attenuated by NPs [109].

Besides pure DPPC and clinical pulmonary surfactant, the mixtures of DPPC and other phospholipids or fatty acids have also been utilized to explore the interaction with PM. These observations can not only shed light on physiological processes but also validate the functions of each component in natural surfactant. In the investigation of surfactant comprised of different combinations of lipids (DPPC, DPPC: POPG, DPPC: DLPC, Infasurf), the POPG-containing lipids showed a significant decrease of alkyl tilt angle in grazing incidence X-ray diffraction (GIXD) measurement when interacted with nanoparticles, meaning that anionic POPG could cause a change in the ratios of LE and LC phases due to the fluidizing property of POPG [127]. POPG is manifested to be less ductile than DPPC at certain surface areas, due to its smaller head group/chain mismatch [171]. Stachowicz-Kusnierz *et al.* [112] compared DPPC, POPC monolayers, and a monolayer of a mixture of DPPC

and POPC. The Π-A isotherms of both the binary monolayer and pure POPC monolayer showed larger mean molecular areas than that of DPPC because of the double bond in POPC. Upon the addition of Benzo [a]pyrene, the condensing effect became more obvious on the binary monolayer than on the one-component monolayers. Molecular dynamics simulations validated this difference by demonstrating that the unsaturated lipids such as POPC and POPG could make surfactant more fluidized, and meanwhile, they might sustain a larger pressure increase at low initial pressure [79,112]. Zhao et al. [109] found that unsaturated lipids DOPC displayed a synergistic solubilization effect with DPPC to increase the total solubilizing ability of natural pulmonary surfactant on PAHs particles.

Monolayers have been extensively investigated, while bilayers and multilayers which exist in a variety of locations in the lung are observed and studied more recently. The bilayer vesicles in the subphase of alveoli and attached to the interface are responsible for the transfer and preformation of the film at the air/water interface. Moreover, more and more evidence revealed that the structure of a surface monolayer with one or more bilayers underneath exists at the alveolar interface. This multi-layered structure which may derive from the multilaminations during the production and migration of lamellar bodies also contributes to the mechanical property of pulmonary surfactant [172]. It has been reported that invading particles also interact with bilayer vesicles during the deposition on the alveoli [97,173]. A dynamic simulation showed that the mean square displacement of dibenz[a,h]anthracene particles on a DPPC/DPPG/cholesterol bilayer (64:64:2) was larger than that on a pure DPPC bilayer, suggesting the important roles of cholesterol and DPPG in the modulation of the flexibility of bilayers [111]. In a broncho-alveolar lavage fluid (BALF), oxides particles interacted with liposome-like structures to form large agglomerates. Instead, the oxides particles interacted with bilayer vesicle structures and formed much smaller aggregates in the 2:1 mixture of DPPC and dipalmitoyl phosphatidic acid (DPPA) [97]. In solutions of unilamellar lipid vesicles composed of DPPC/POPG/Palmitic acid (PA), Ruge et al. [174] discovered that the lipids greatly modulated the effects exerted by SP-A and SP-D which enhanced the alveolar macrophage uptake of magnetite nanoparticles.

When a cationic lipid such as cetyltrimethylammonium bromide (CTAB) was added to DPPC monolayer, the bulking of the monolayer was diminished at high surface pressure. This result is due to the cohesive effect of CTAB that enables the monolayer to maintain flat geometry and even achieve negative surface tension at high surface pressure [175].

4.3. Studies of surfactant interacting with different PM

4.3.1. The effect of particle size

It is known that particle size impacts the cellular uptake of particles. *In vivo* studies indicated that larger NPs caused a greater load of macrophages [176] and induced more cytotoxicity and inflammation in mice [177]. Particle size also plays a crucial role in the interactions between PM and lung surfactant. In a study of poly(organosiloxane) NPs with diameters of 12 nm and 136 nm [165], 12 nm particles did not cause

significant changes on the isotherm curves of both DPPC monolayer and DPPC/DPPG/SP-C (80:20:0.4 mol %) lipid mixture except at very high concentrations, while 136 nm particles diminished the coexistence of LE and LC in DPPC monolayer but enhanced the transition plateau of DPPC/DPPG/SP-C film even with low concentrations. The isotherm of DPPC monolayer, in this case, did not shift to larger molecular areas with nanoparticles, suggesting the transfer of some lipid molecules to particle surface. The compressibility of both DPPC and the mixture films was increased with the presence of 136 nm particles, resulting from the perturbed lipid packing order and decreased intermolecular interactions. These effects were stronger with higher particle concentrations. The disturbance on the interfacial packing is controlled by an interplay between steric hindrance, excluded area effects and other interactions [178]. The large particles also attenuated the phase separation of DPPC monolayer due to the decrease in line tension and inhibited the vesicle insertion process, which would impair the preformation of surfactant interfacial film [165].

Nevertheless, the strength of particle-surfactant interaction is not linearly associated with particle size. Instead, parabolic curves are always derived with the existence of critical diameters that cause a significant change in the biophysical properties of pulmonary surfactant, and the values vary with the type of NPs. Ku et al. [179] reported that the isotherm of DPPC monolayer shifted to larger molecular areas when interacting with gelatin-based particles (136 nm, 197 nm, 221 nm, 236 nm, 287 nm). The extent of the shift was maximum with the 236 nm particles. The surface potential of the DPPC film was also greatly influenced by the presence of the particles, thereinto smaller particles resulted in steeper and less delay of the headgroup dipole reorientation while larger particles led to stronger delay. Kodama et al. [130] discovered that among the five different sizes, only 20 nm particles led to the disappearance of "squeeze out" plateau of Survanta, which was also verified in the fluorescence microscopic image showing that only the 20 nm particles caused changes in the LC domain. A molecular dynamic simulation was conducted by Curtis et al. [173] to explore how different sized particles interact with DPPC bilayers. The results indicated that the hydrophilic particles with diameters from 2 nm to 25 nm became wrapped in DPPC bilayer, while smaller particles with 1 nm diameter were embedded in the bilayer surface (Table 3). Equation (21) shows the equation denoting that the radius of particles influences the wrapping energy of the particles in lipid membrane:

$$E = \left(2\epsilon/R^2 + \text{в} - u_{ad} \right) A_c \tag{21}$$

where ϵ is the membrane bending rigidity, R is the radius of particles, в is the membrane tension, A_c is the contact area, u_{ad} is the adhesion energy per unit area [180].

Kodama et al. [130] pointed out that the effect of particle size on particle-surfactant interaction might be ambiguous since the observation would also partly result from the difference of the associated physical properties, e.g. total surface area and specific surface area, the chemical nature of particle-molecule interaction. The total surface area effect has already been evaluated and it was excluded from the factors

Table 3
Particle size effects on particle-surfactant interaction

Author/year	Particle composition	Size range	Surfactant	Main findings
Ku et al./2008 [179]	Gelatin particles cross-linked with glutaraldehyde	137, 197, 221, 236, and 287 nm	DPPC monolayer	236 nm particle has the highest affinity towards surfactant
Dwivedi et al./2014 [165]	Poly(organosiloxane)	12nm and 136nm	DPPC monolayer and DPPC/DPPG/SP-C (80:20:0.4 mol%)	Severe inhibition only observed with 136 nm particle
Kodama et al./2014 [130]	Polystyrene	20, 30, 40, 100, 500, and 1000nm	Survanta	Only 20 nm particle eliminates the squeeze-out phase in isotherms and drastically increases the domain fraction of the LC phase
(Simulation) Curtis et al./2015 [173]	Coarse-grained nanoparticles	1, 2, 4, 6, 10, and 25nm	Coarse-grained DPPC bilayer	Hydrophilic particles larger than 2 nm become wrapped while 1 nm particles become embedded
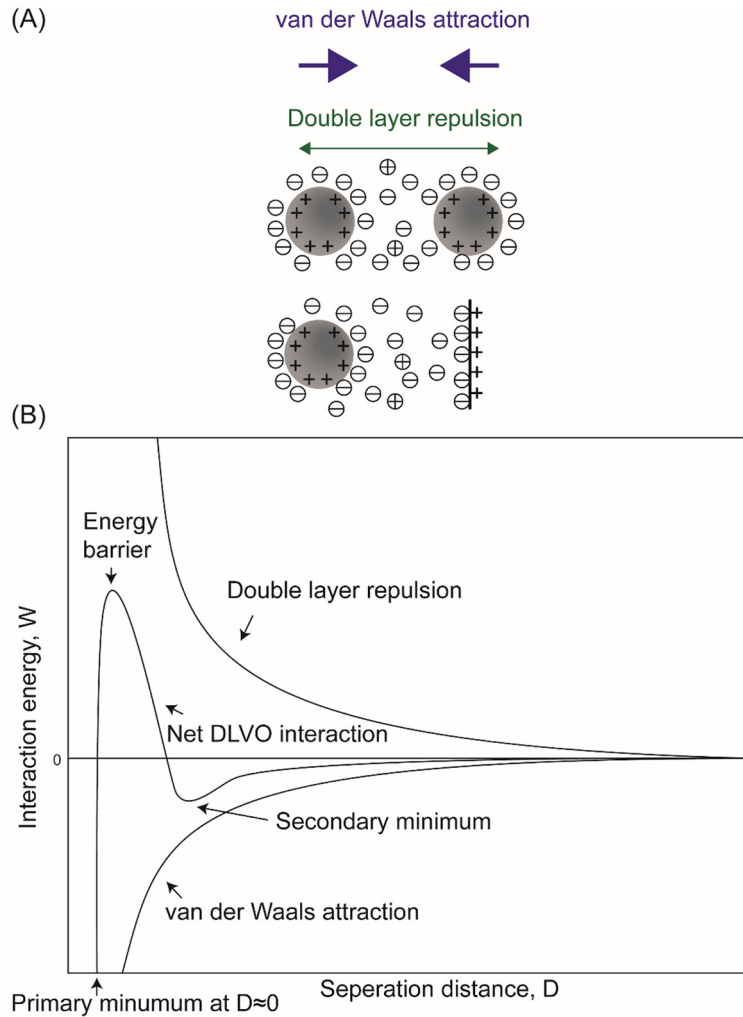
Fig. 6. (A) Schematics of DLVO interactions between positively charged particle-particle and particle-surface systems in an aqueous solution. For surfaces carrying similar charges in the aqueous media, their DLVO interactions combine the effect of electrical double layer repulsion and van der Waals attraction. (B) Schematic plots of DLVO interaction energy vs. separation distance between similarly charged surfaces or colloidal particles dispersed in aqueous solutions. The double layer force exists as relatively long-rang repulsion. The net DLVO interaction has a high peak known as the energy barrier at high charge density and low electrolyte concentration. In concentrated electrolyte solution, a secondary minimum would appear at some critical separation, while the primary minimum is present when the interacting surfaces are in contact. When the surface charge densities are high in solutions with dilute electrolytes, the surfaces repel each other as the double layer force dominates. When the charge densities are below a certain value or the electrolyte concentration is higher than the critical coagulation concentration, the energy barrier falls below 0, giving rise to rapid coagulation [188].

impacting the phase transition of surfactant. However, the researches on the effect of specific surface area and nature of particle-molecule interaction are limited. In general, particle size can only be assessed as a reference factor, rather than an independent factor that determines the particle-surfactant interaction.

4.3.2. The effect of surface charge

Surface charge is a key factor determining the toxicity of NPs. The study of functionalized (e.g., Guanidinium-, acetylated-, zwitterionic-, hydroxylated-, PEGylated-, carboxylated- and sulfated-) polystyrene particles proved that lung inflammation was significantly influenced by surface charge [181]. Regarding the interactions between particles and pulmonary surfactant, electrostatic force has been considered as one of the main contributors [96,99,182]. Electrostatic force is a much stronger and longer-range force than other forces [183]. According to Coulomb's law, the electrostatic force K_E, between two charged particles is

$$K_E(\mathbf{d}) = \frac{Qq\hat{\mathbf{d}}}{4\pi d^2 \varepsilon_0 \varepsilon} \tag{22}$$

where Q and q are the charges of the particles respectively, $\hat{\mathbf{d}}$ is the unit vector from one particle to the other, d is the distance between the particles, as

$$\hat{\mathbf{d}} = \mathbf{d}/|d| \tag{23}$$

ε_0 is the vacuum permittivity and the approximate value is 8.85×10^{-12} $C^2N^{-1}m^{-2}$. ε is the dielectric constant of the medium. The electrostatic force would be attractive if Q and q are of opposite signs, otherwise repulsive.

When taking the aqueous environment (e.g., the subphase) into consideration, the effect of surface charge becomes more complex. According to the Derjaguin-Landau-Verwey-Overbeek (DLVO) theory, the interaction between charged spherical PM and surfactant surface is influenced by both the van der Waals force and double layer force which derives from the electric double layer formed in aqueous solutions [184–186]. An equation describing the double layer force between a charged sphere and a flat surface is given as

$$F_{double} = \frac{2\pi R}{\varepsilon_l \varepsilon_0 \kappa} \left[(\sigma_T^2 + \sigma_S^2) e^{-2\kappa d} + 2\sigma_T \sigma_s e^{-\kappa d} \right] \tag{24}$$

where R is the radius of the sphere, ε_l and ε_0 are the dielectric constant of the liquid and vacuum, respectively, κ is the inverse of the Debye length, σ_T and σ_s are the surface charge densities of the sphere and the surface, respectively [187]. Fig. 6 illustrates a DLVO model for the particle-particle and particle-surface systems with same charge signs as an example. The double layer force exhibits as repulsive in this case. Besides van der Waals force and double layer force curves, a net DLVO interaction curve is also plotted. For PM-lung surfactant surface system, double layer force may exist as repulsive or attractive, depending on the charge sign and charge density of PM, and the composition of lung surfactant. The surface charge densities and electrolyte concentrations determine the magnitude of the energy barrier, reflecting the stability of the particle-particle dispersion and particle-surfactant film system in the solutions.

The silica particles with negative charges form lipid-particle complexes with the positively charged ammonium groups of DPPC, changing the dipole moment of the DPPC molecules to affect the molecular packing, thus the nucleation of LC domains is disrupted. As a result, the LE-LC plateau on the isotherm becomes flat [189]. Another negatively charged particles - carboxyl modified polystyrene caused a partial collapse of the DPPC monolayer and changed the ratio of ordered domains to obtain a more compact DPPC monolayer. The polystyrene particles also increased the hysteresis area during compression and expansion cycle. These phenomena proved the adsorption of the polystyrene particles to DPPC during expansion and the ejection of the particles to subphase during compression [134]. The electrostatic interaction also greatly eliminates the translocation capability of particles and the elimination effect increases with surface charge density. In a molecular dynamics simulation, the charged particles were partially wrapped in DPPC instead of penetrating the film, facilitating the structural change and inhibiting the phase change of the surfactant film (Fig. 7C, D, E) [190].

The positively and negatively charged particles do not show much difference to pure DPPC due to the zwitterionic property of the molecules. However, because of the presence of other cationic, anionic lipids and proteins in natural pulmonary surfactant, the effect of particle charge becomes complex (Fig. 7A). Negatively charged polylactide nanoparticles were found to be a more potent surface activity inhibitor on Curosurf than positively charged nanoparticles [104]. Hu *et al.* [191] confirmed this trend in a molecular dynamics simulation. It is because that the positively charged SP-B$_{1-25}$ could be adsorbed onto the anionic particles even when the anionic particles were trapped in the film, leading to protein denaturation and the conformational change of surfactant. Another positively charged protein SP-C also contributes to this effect [92,104]. However, in the investigations of aluminum oxide, silicon dioxide, and latex nanoparticles, the negatively charged latex and silica did not cause direct or strong interaction to either synthetic (mixture of DPPC, POPG, etc.) or exogenous surfactant (e.g., Curosurf), while the positively charged aluminum oxide, silica and latex form aggregates with surfactant vesicles, and the interaction strength increased with surface charge density. The particle-vesicle aggregates can last for weeks [101]. This affinity of positive particles towards lung surfactant is ascribed to the net negative charge of the surfactant. Behyan *et al.* [127] reported that both cationic and anionic silica particles shifted the isotherms of DPPC: POPG to larger molecular areas with low concentrations in the subphase, while only cationic particles showed an impact on Infasurf isotherm at high surface pressure. However, though GIXD and x-ray reflectivity studies revealed that anionic silica nanoparticles would interact with lipid head and change the alkyl chain organization and orientation of the surfactant, the effect was very small. By contrast, cationic nanoparticles caused a large reduction of the chain tilt angle in the condensed phase, which would affect the LE-LC phase ratio, thus changing the mechanical properties of the film (Fig. 7B). Behyan's discovery was believed to be strongly associated with the presence of anionic

POPG. The interactions caused by the introduction of anionic particles observed in some other studies were from the electrostatic repulsion between the anionic phospholipids and the particles [192].

In general, the surface charge of particles enhances the interaction with lipids. For pure DPPC monolayer, because of the zwitterionic feature, the charge signs of particles do not make much difference on the translocation behaviors [190]. The behavior is quite different in natural pulmonary surfactant with the presence of other lipids and surface proteins, where positively charged particles always cause more pronounced effects on the structural and functional properties of the surfactant. The strength of the interaction is positively related to surface charge density. However, Kodama claimed that the effect on particle-surfactant interaction brought about by surface charge was not as powerful as that of particle size [130].

4.3.3. The effect of particle hydrophobicity

Besides electrostatic attraction, hydrophobicity also contributes to the interaction between PM and lung surfactant. Hydrophobic interaction is greatly dependent on temperature since it is entropy-driven. The entropy will increase ($\Delta S > 0$) when hydrophobic particles interact with each other, while the enthalpy decreases ($\Delta H > 0$) resulting from the breaking of hydrogen bonds. According to Gibbs free energy formula

$$\Delta G = \Delta H - T\Delta S \tag{25}$$

if ΔH is smaller than $T\Delta S$, it leads to a negative value of ΔG, which indicates the spontaneous hydrophobic assembly. There is no widely accepted theoretical formula for hydrophobic force or energy because the interactions between macroscopic hydrophobic surfaces and those between hydrophobic nanoparticles or molecules are not quantitatively equal. For example, the hydrophobic interaction between two solid surfaces could be demonstrated in Eq.(26) [193]

$$\frac{F_{HB}(D)}{\lambda} = -C_0 e^{-D/D_{HB}} \tag{26}$$

where λ is the curvature of the interacting surfaces, C_0 is an empirical parameter, D is equilibrium distance, D_{HB} is the hydrophobic decay length. An empirical formula showing the hydrophobic energy is

$$E_{HB} = -\gamma(a - a_0)e^{-D/D_{HB}} \tag{27}$$

Here, γ is the interfacial tension, a is the area per molecule, a_0 is the optimum area per molecule [194]. Additionally, the existence of hydrophilic headgroups, tails and other moieties, and local surface geometry also directly affect the hydrophobic interactions. Therefore, hydrophobic force is non-additive [195]. As a matter of fact, the long-range force observed between two hydrophobic objects is a combination of several forces [196]. Hydrophobic force predominates over electrostatic and steric repulsion when the distance of the particles decreases to the decay length [194]. The calculated energy curves in Fig. 8 indicate that hydrophobic interaction is a short-range force.

Hydrophobic particles can nucleate the collapse of the compressed DPPC monolayer, causing an irreversible decrease of the collapse pressure, as hydrophobic attraction leads to the formation of particle-DPPC complex and stabilizes the particle-DPPC monolayer from expelling the particles [189,197], which contrasts the observation on hydrophilic silica particles [178]. This trend is also supported by Zhang *et al.* [106] that the aggregates formed by the introduction of hydrophobic Au NPs to disturb the domain size on DPPC monolayer could stay on the surface of pulmonary alveoli for a long time. It is owing to the hydrophobic interaction between the Au particles and the surfactant, and this interaction decreased the compressibility and inhibited the phase transition of the surfactant. The retention rate of hydrophobic particles at the surfactant Infasurf monolayer is also higher than that of hydrophilic particles (Fig. 9A) [198]. It is the acyl group [165] as well as the long hydrophobic tails [199] of DPPC molecules that interact with hydrophobic particles,
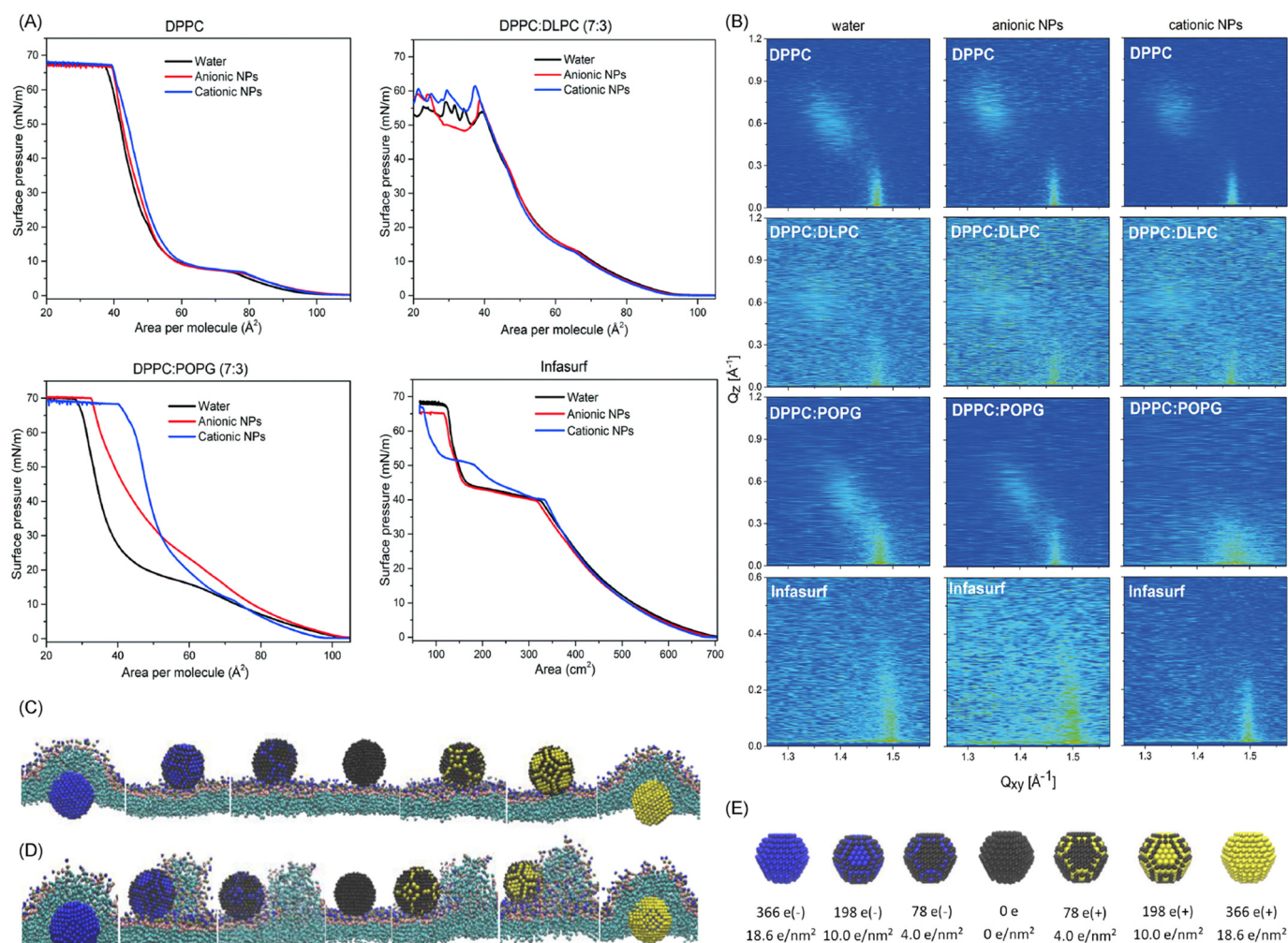
Fig. 7. (A) Surface pressure-area isotherm and (B) contour plots of x-ray intensities vs. in-plane and out-of-plane scattering vector components q_{xy} and q_z of various surfactant systems with and without NPs silica Levasil 200S (cationic) and Bindzil 30/360 (anionic). The surfactant mixtures are DPPC: DLPC (7:3 by mole ratio) and DPPC: POPG (7:3). (A) The introduction of NPs did not cause significant changes in DPPC and DPPC: DLPC. Both cationic and cationic NPs caused an increase in the molecular area of DPPC: POPG, while only cationic NPs shifted the Infasurf curve at the pressures above the "squeeze out" plateau. (B) The systems were treated as homogeneous monolayer based on the assumption that the sizes of LE and LC domains are smaller than the x-ray beam footprint. The diffraction peaks of DPPC, DPPC: POPG and Infasurf shifted to larger value of q_z with anionic NPs, revealing a unit cell expansion. Cationic NPs induced the shift of the diffraction peaks in DPPC: POPG and Infasurf to lower q_z, indicating a reduction in the tilt angle. The subphase for each sample was ultrapure water (left), anionic silica NPs aqueous solution (middle), and cationic silica NPs aqueous solution (right). Surface pressure: 35 mN/m; in (A) and (B), the concentrations of NPs were 0.001 wt%. Temperature: $22.0 \pm 0.5^\circ C$ [127]. Republished with permission of Royal Society of Chemistry, from "Nanoparticle-induced structural changes in lung surfactant membranes: an X-ray scattering study", Behyan *et al.*, 5, 2018 [127]; permission conveyed through Copyright Clearance Center, Inc. (C) (D) (E) Molecular dynamic simulation. Hydrophilic NPs with positive and negative charges interact with pulmonary surfactant monolayer [190]. (C) is at expanded state and (D) is at compressed state. Each column shows the final structure of the particle-surfactant interaction corresponding to surface charge density. The upper side of the monolayer is water and the lower side is air. (E) The model of NPs set up in the simulation. The surface charges and densities are illustrated. Color code: the neutral coarse-grained beads in black, the cationic in yellow and the anionic in blue. It showed that the charged particles were only wrapped in the monolayer instead of directly penetrating. Republished with permission from "Effect of the surface charge density of nanoparticles on their translocation across pulmonary surfactant monolayer: a molecular dynamics simulation", Chen *et al.*, Molecular Simulation, 2018 [190], published online on 25 Jun 2017. Reprinted by permission of the publisher (Taylor & Francis Ltd, http://www.tandfonline.com).

therefore DPPC molecules would be adsorbed to particles from the air/water interface, changing the structure of the surfactant monolayer. Konduru *et al.* [97] discovered that the lipid adsorption ability of hydrophobic cerium oxide was much stronger than that of other hydrophilic particles when incubated in different surfactant systems including DPPC, DPPC/DPPA, and rat bronchoalveolar lavage fluid (BALf) (Fig. 9B).

The Π-A isotherm of DPPC was significantly and horizontally shifted to larger molecular surface areas by hydrophobic montmorillonite and silica particles owing to the formation of hydrophobic complexes with the incorporation of the particles, which led to excluded area effects [129,197]. The hydrophilic halloysite and bentonite NPs shifted the Π-A isotherm to smaller molecular areas, resulting from

the decreased distance between DPPC molecules [129]. In Infasurf, the effect of particles on isotherm is a little bit different. Both hydrophilic and hydrophobic particles shifted the curve to smaller surface areas, increasing the compressibility of the film, as well as decreasing the ability to reduce surface tension upon compression and inhibiting the compression-expansion activity (Fig. 10A, B) [191,198]. It is proposed that hydrophilic particles can bind to the polar end of DPPC molecules, leaving the hydrocarbon tails pointing out. This attraction also causes the adsorption of lipid molecules to hydrophilic particles, and the lipid-particle complexes would further aggregate to sink [129], though this adsorption is not as strong as that driven by hydrophobic interactions [97]. When incubated in the mixture of DPPC and
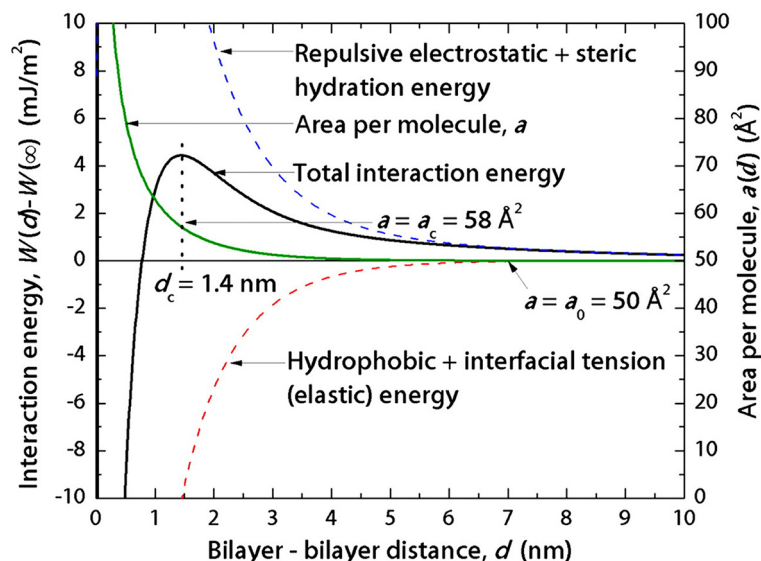
Fig. 8. The overall force law of interaction energies and individual contributions vs. separation distance for trans azobenzene trimethylammonium bromide (azoTAB) bilayers. The hydrophobic energy is dominating as the bilayer-bilayer distance deceases to about 1 nm, indicating that the force between hydrophobic objects becomes pure hydrophobic interaction at short range [194]. Republished with permission from Donaldson et al. [194], Proceedings of the National Academy of Sciences, 2011; 108: 15699.

DPPA, hydrophobic particles would insert into lipid vesicles and be associated with the formation of multilamellar lipid bilayers, while the relatively hydrophilic ones stayed outside lipid bilayers vesicles and related to the formation of unilamellar lipid bilayers (Fig. 9B) [97]. The translocation behaviors that were studied by molecular dynamics simulations showed that both hydrophilic and hydrophobic particles would transport through the surfactant, but in different manners. The hydrophilic particles directly penetrated the monolayer, while the hydrophobic particles were wrapped by the surfactant and passed through the DPPC monolayer [200]. For DPPC bilayer, the hydrophobic particles directly penetrated the membrane and were embedded within the inner hydrophobic core of the bilayers, while hydrophilic particles became wrapped by the lipid bilayers [173]. The combined in vitro and in silico research conducted by Hu et al. [191] on Infasurf suggests that hydrophobic polystyrene particles caused the formation of high protrusions as the film was compressed, resulting from the encapsulation of the particles, while hydrophilic hydroxyapatite particles translocated quickly across the film. Hu also revealed that the
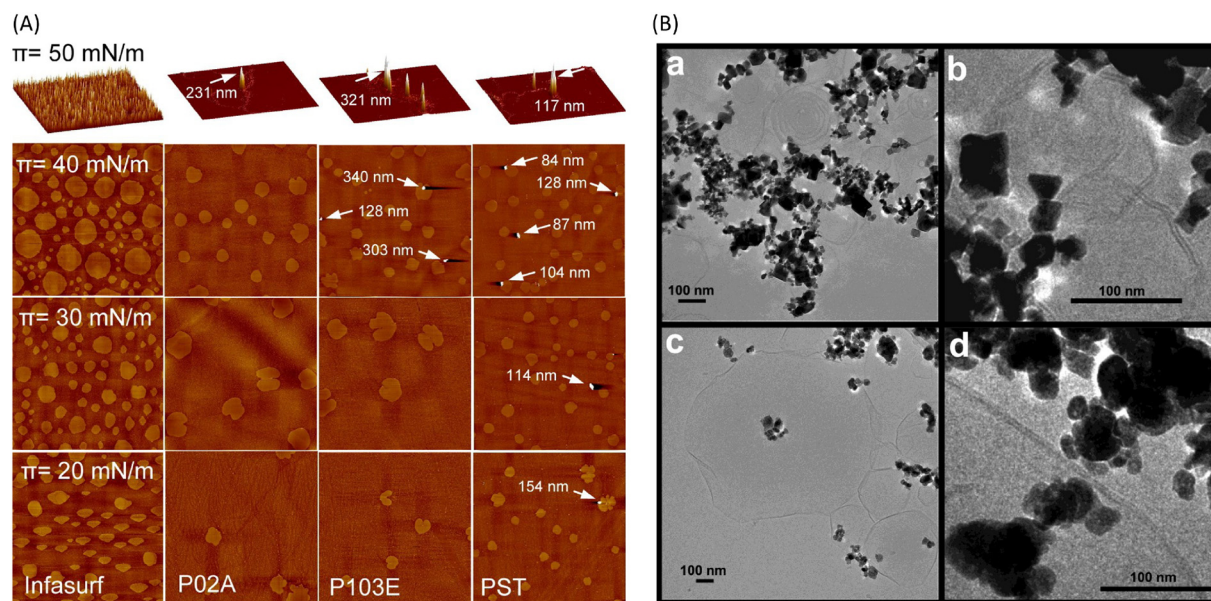
Fig. 9. (A) Comparison of NPs retention at the Infasurf film. AFM images of pure Infasurf and Infasurf mixed with NPs at four different surface pressures (20, 30, 40, and 50 mN/m). P02A: acid-terminated poly(D,L-lactide-co-glycolide) (PLGA), P103E: ester-terminated PLGA, PST: polystyrene. The hydrophobicity increases as a manner that P02A is the least hydrophobic, P103E is the medial and PST is the most hydrophobic. The resolution of AFM images at 20, 30, and 40 mN/m is 50μm*50μm and the z range is 5nm. The resolution of AFM images at 50 mN/m is 20μm*20μm, z ranges are: Infasurf, 20 nm; Infasurf + P02A, 250 nm; Infasurf + P103E, 350 nm; and Infasurf + PST, 120 nm. The image at 50 mN/m is depicted in 3D. NPs are indicated with white arrows. The presence of NPs is positively related to hydrophobicity. After the monolayer-to-multilayer transition, all three types of NPs are spotted at the surface [198]. Reprinted with permission from Valle et al. [198]. Copyright (2014) American Chemical Society. (B) Cryo-TEM images of 2:1 mixture of DPPC: DPPA with particles CeO_2 (a,b) and $BaSO_4$ (c,d) [97]. NPs interacted with lipid vesicles with polyhedral shapes. Onion-like multilamellar vesicle structures were present with CeO_2 while unilamellar vesicles were shown with $BaSO_4$. Reprinted with permission from Konduru et al. [97]. Copyright (2018) American Chemical Society.

(A)

(B)

(C)
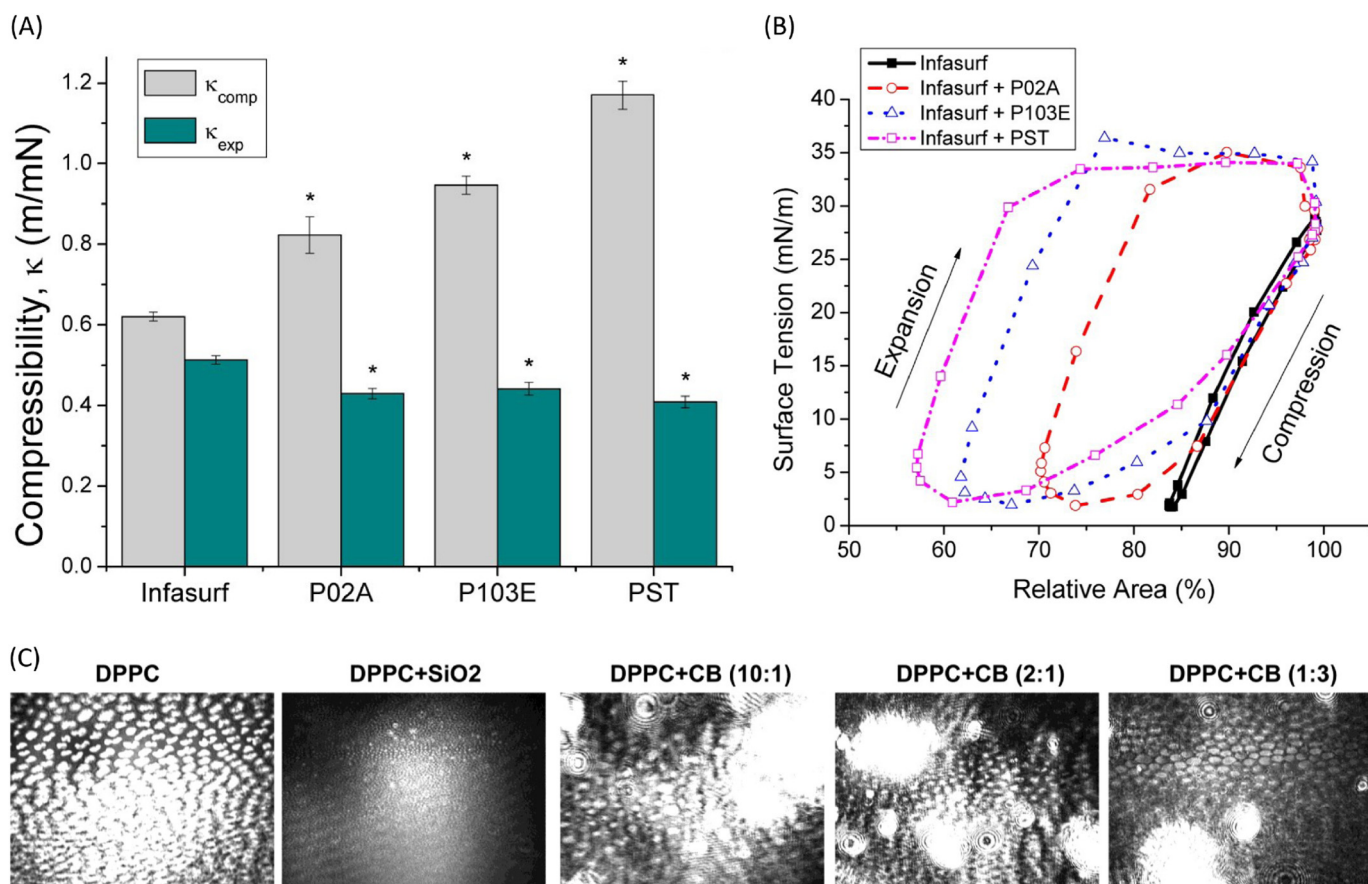
Fig. 10. (A) Statistical analysis of the effect of NPs on the compressibility of Infasurf. *p < 0.05 for comparison to pure Infasurf. NPs significantly increased the compressibility during compression (κ_{comp}) and decreased the compressibility during expansion (κ_{exp}). The extent is proportional to hydrophobicity. (B) Compression and expansion cycles for pure Infasurf and Infasurf with NPs. The hysteresis area was increased with NPs and the extent increased with hydrophobicity. (A)(B) The data were obtained with constrained drop surfactometer at 37°C and cycled at a physiological relevant rate (3s/cycle). P02A: acid-terminated PLGA, P103E: ester-terminated PLGA, PST: polystyrene. The hydrophobicity increases as a manner that P02A is the least hydrophobic, P103E is the medial and PST is the most hydrophobic [198]. Reprinted with permission from Valle et al. [198]. Copyright (2014) American Chemical Society. (C) BAM images (311 μm*418 μm) of pure DPPC on pure water subphase, and DPPC on SiO₂ (1 wt %) and carbon black (CB) dispersions at Π = 7.5 mN/m. Compared with CB, the stronger distorting effect on the domain size and shape caused by SiO₂ is mainly from electrostatic attraction [189]. Reprinted with permission from Guzmán et al. [189]. Copyright (2011) American Chemical Society

inhibition induced by hydrophobic polystyrene particles to Infasurf is faster than that caused by hydrophilic hydroxyapatite particles. However, the hydrophobicity of particles does not cause much difference when interacting with the hydrophobic SP-A and hydrophilic SP-D. These two surfactant proteins are selectively adsorbed to the particle and interplay with the lipids, hence the alveolar macrophage uptake of hydrophobic and hydrophilic particles in the unilamellar vesicles are at comparable levels [174].

Though previous studies on natural pulmonary surfactant such as Survanta [199], BALF [97] indicated that some lipids could be adsorbed onto the hydrophobic particles via strong hydrophobic interactions, there was no significant change in the domain formation and structure of Survanta after the introduction of particles in Tatur's experiments, which was speculated due to the merging of the particles into the hydrophobic surface proteins existed in the natural surfactant [108]. However, Valle et al. [198] observed that the size of the phospholipid domains of Infasurf was reduced by both hydrophilic and hydrophobic NPs, along with the disturbance on the conformational monolayer-to-multilayer transition. This difference is due to the particle size. In the former study, the particles with core diameter of 2 nm were comparable to the size of SP-B and SP-C and easily accumulated with these hydrophobic proteins in the LE phase; while the sizes of particles in the latter experiment were 260, 350, and 95 nm which led to the formation of protrusions on the monolayer.

Both hydrophobicity and surface charge play important roles in the phase behavior and structure of pulmonary surfactant, whereas the disrupting effect of surface charge is related to electrostatic interaction, which influences the orientation of DPPC molecules. Thus the surface charge always causes stronger effects on the biophysical properties and domain structure of DPPC (Fig. 10C) [189]. Nevertheless, the amount and type of lipids adsorbed onto the particles are determined by hydrophobicity rather than surface charge [97].

4.3.4. The effect of particle shape

Kondej et al. [129] noticed that the particle shape also led to differences in the phase behavior of DPPC. Plate-like bentonites and halloysite nanotubes showed different impacts on the phase behavior of DPPC, despite that they are all hydrophilic and surface-inactive. The dissimilar behaviors of the bentonite and halloysite particles compared with spherical silica particles suggest that the squeezing-out of particle-lipid complexes during compression was amplified for the non-spherical particles [129,189]. A systematic molecular dynamics study has been conducted to validate the influence of particle shape. For hydrophilic particles, the simulation showed that they penetrated DPPC monolayer, but the rod particles seldom disrupted the packing structure of DPPC while the barrel and disk particles caused an obvious change in the structure. Barrel particles led to the most obvious disturbance because of the largest contact area, while rod particles

showed the smallest contact area with DPPC molecules to induce the lowest influence. Shape also affects the penetration ability as the rod-like particles bore the highest penetration ability. This simulation suggests that the length-to-diameter aspect ratio of cylindrical NPs is the key parameter to determine the penetration ability of particles and structural disturbance on DPPC monolayers [201]. Kondej *et al.* [169] examined the influence caused by nanotubes and nanohorns, the results showed that the nanomaterials with higher specific surface areas induced more frustration to lung surfactant. Capillary force is speculated as one of the reasons why particle shapes influence the particle dynamics and disruption of lung surfactant. The capillary force is higher for the particles with sharper edges because of the pinning of the air-water interface at the edges, especially for cylindrical or cubical shapes [202,203].

In conclusion, the strength of capillary force increases with the length of air-water-solid interface [203]. Besides, shape anisotropy and the initial orientation of particles also contribute to the shape effects on particle-lipid interaction [204].

4.3.5. The effect of adsorbates, ambient dust and other polymer composites

PM carries many different kinds of chemicals. One of the most toxic components in PM is polycyclic aromatic hydrocarbon (PAHs) which has been proved to cause carcinogenic effect to organisms. Several recent papers have discussed the interactions of some PAHs with pulmonary surfactant. Zhao *et al.* [109] revealed that natural surfactant increased the solubilization of anthracene significantly, depressing the adsorption of anthracene to nanoparticles, thus the adsorption of anthracene to pulmonary surfactant was enhanced, which led to increased toxicity of the inhaled particles. Zhao *et al.* [205] confirmed that the mixed phospholipids in natural surfactant were responsible for the solubilization of PAHs. A molecular dynamics simulation [112] and experimental results [76] indicated that benzo[a]pyrene caused a condensing effect on surfactant monolayer and reduced the hydration of the monolayer, leading to a decreased fluidity. Benzo[a]pyrene also destabilizes DPPC/DPPG monolayer by decreasing the surface pressure. Nevertheless, during compression, benzo[a]pyrene may be expelled to water subphase due to the presence of DPPG. These results suggest that the accumulation of benzo[a]pyrene in surfactant monolayers not only impairs the surfactant function but also attenuates the barrier role of the surfactant with an easier access to the underneath fluid [76]. Another simulation about dibenz[a,h]anthracene and its metabolite 3,4-diol-1,2-epoxide interacting with lung surfactant bilayers showed that they formed aggregates in the lipids and subphase, as well as at the interface. The metabolite was more likely to diffuse through the film to the subphase [111].

Besides pure synthetic compounds, some complex PM derived from ambient dust including tobacco smoke, diesel exhaust dust, biofuel combustion dust, etc. have also been investigated with lung surfactant and the models. The particle emissions from biofuel combustion were revealed to deposit in alveoli, increasing the compressibility of lung surfactant and lowering the surface pressure, thus destabilizing the monolayer. Meanwhile, the particles can also predispose the collapse of alveoli, leading to respiratory distress [114]. Sosnowski *et al.* [110] revealed that benzo[a]pyrene released from soot particles interacted with the hydrophobic part of lung phospholipids and inhibited the dynamic and mechanical properties of lung surfactant. The pulmonary clearance rate was also reduced. Kendall reported that a lot of DPPC and amino acids in bronchoalveolar lavage were adsorbed to urban PM$_{2.5}$ particles, which would sequester the lung surfactant [115]. Electronic cigarettes are used as an alternative to cigarettes, but a high concentration of the major adsorbate glycerol and propylene may induce a decrease in the surface tension and hysteresis of the surfactant during compression. This effect would be more obvious in people who have already had lung diseases [206]. The side effect caused by ambient PM is not easy to be overcome by lung surfactant, as the inhibition gets stronger with time, leading to alveolar atelectasis [114]. Moreover, the adsorption of surfactant components to PM would interfere with innate immunity [115].

Polymeric materials have been utilized in industry in huge amounts, and as a result, ambient PM contains increasing amounts of polymeric particles. Moreover, as a popular platform in the application of nanomedicine, the potential toxicity of polymeric materials has become a concern. Chitin[poly(b-(1-4)-N-acetyl-D-glucosamine)] is a biopolymer that has been utilized in food, cosmetics and pharmaceutical industries due to its biocompatibility. Recent papers showed that chitin would affect the structure and function of lung surfactant by electrostatic attraction. Chitin could adsorb the phospholipids, hindering the formation of LC phase. Under higher pressure, the chitin particles were squeezed out along with some adsorbed lipids, thus the order of the monolayer was disturbed [207]. Poly(styrene) and poly(lactide) are two common polymers that have been applied in nanomedicines. However, these polymers always provoke a decrease in lung activity by aggregation and protein depletion [131,208]. These adverse effects can be resolved with coatings. For example, poloxamer and bioinspired poly (2-methacryloyloxyethyl phosphorylcholine) coatings can prevent particle aggregation and the adsorption of surfactant to particles by steric shielding, thus the impairment of the biophysical functions can be significantly attenuated [105,208,209]. The exploration of the interaction between various polymers and pulmonary surfactant could provide inspiration to the development of lung drug delivery platforms with high biocompatibility and low toxicity.

5. Health Effects Associated with PM invasion

When PM readily interacts with pulmonary surfactant and deposits on it, besides physical properties, physiological properties of the surfactant are also influenced. PM penetrates through the surfactant into lung epithelial cells and causes further physiological disturbance to lung and other organs [210]. It is speculated that bone marrow can be stimulated by PM deposition and cause systemic inflammatory response, leading to chronic diseases such as cardiovascular disease, because cytokines were detected in the circulation in response to PM [211]. It is also hypothesized that nanoparticle is able to penetrate through epithelial into the circulation directly and cause diseases, since the inhaled particles were found at the sites of vascular disease [212].

In addition to PM and the toxic chemicals adsorbed to PM, another type of adsorbate on PM-microorganisms can also strongly affect human health. A two-day exposure to high levels of PM$_{2.5}$/PM$_{10}$ significantly changed in the composition of the pharyngeal microbiota [213]. Compared with pre-smog swabs, the relative abundance of 38 phyla, including *Firmicutes, Fusobacteria,* and *Actinobacteria*, increased in post-smog swabs. Among them, *Leptotrichia, Corynebacterium* and *Veillonella* were the top three genera with more than 20,000 reads for each. In addition, there were 11 new phyla detected in post-smog swabs. This change may increase unexpected risks, especially respiratory infections, to human. It should be noted that the relative abundance of two respiratory pathogens *H. influenza* and *M. catarrhalis* were increased by 240% and 150%, respectively, which would lead to morbidity and mortality of diseases such as pneumonia. Influenza A virus significantly changed the metabolism of alveolar type II cell in surfactant lipid, leading to surfactant dysfunction [214]. Coronavirus SARS-CoV-2 that triggered the current pandemic could damage both type I and type II alveolar cells, giving rise to reduced production and secretion of pulmonary surfactant to the alveolar interface, as well as inhibiting gas exchange between blood and the alveoli. Middle East respiratory syndrome (MERS)-CoV could also infect type I cells [215].

5.1. Physiological effects on pulmonary surfactant

Schürch *et al.* [216] reported in 1990 that the latex particles deposited in hamster lungs were submerged in the subphase and coated

with osmiophilic film. A direct physiological change of pulmonary surfactant with deposition of PM is the elevation in the amounts of surfactant, which would lead to surfactant dysfunction. Murphy *et al.* [217] discovered that crystalline quartz led to an increase of extracellular surfactant, resulting from the increased number or secretion of type II cells. The augment of single surfactant component was also observed in rat lung with the inhalation of fly ash [218]. In this study, total phospholipids, phosphatidylcholine (PC) and phosphatidylethanolamine (PE) significantly increased in lungs. Meanwhile, PC, especially DPPC in lung surfactant, and microsomes were much higher upon PM exposure. It is due to the CDP-choline pathway and N-methylation of PE in lung cells. Another *in vivo* study on rats exposed repeatedly to diesel exhaust also testified the overproduction of phospholipids in pulmonary surfactant, indicating the risk of chronic lung injury [219]. The production of certain surfactants is a defense mechanism to protect the lung from further injury and avoid alveolar collapse caused by PM [218]. When the pulmonary macrophage fails to clear the increased surfactant, alveolar lipoproteinosis occurs [220], leading to shortness of breath.

Microbial virus adsorbed to PM also induces changes in the composition of lung surfactant. For example, *Pseudomonas aeruginosa* flagellum caused the production of exoproteases to degrade SP-A [221], making the surfactant and the alveoli susceptible to infection. Protease IV secreted by *Pseudomonas aeruginosa* was proved to degrade SP-A, SP-B and SP-D, changing the surface tension-reducing function of the surfactant in addition to the reduction of host defense function [222]. The decrease in SP-B may also lead to the change in the permeability of the surfactant [223], making the membrane more susceptible to PM and the adsorbates. A mucoid strain of *Pseudomonas aeruginosa* decreased the content of DPPC by reducing the mRNA synthesis of phosphocholine cytidylyltransferase (CTP) which is a key enzyme for DPPC synthesis [224], resulting in reduced surfactant function.

5.2. Health effects behind interaction of pulmonary surfactant and PM

5.2.1. Inflammation

It is known that specific PM can deposit and translocate within pulmonary surfactant. Many studies present that both PM and the adsorbates (e.g., microorganisms, metals) on PM can lead to inflammatory response. When PM penetrates through the surfactant, alveolar macrophages can trigger phagocytosis to clear PM, which releases inflammatory mediators such as leukocytes and neutrophils to induce inflammation. Furthermore, the disturbance on the film structures may cause mechanical damage on the surfactant and epithelial cells, which may lead to inflammation as well. The acute effect of PM on living animals and humans mostly shows lung inflammation at first [225]. As the immune system's response to harmful stimuli, inflammation activates cellular and molecular events to remove the stimuli and tries to heal [226]. Inflammation is exhibited as the increase of free cells and high proportion of neutrophils in lavage. Uncontrolled inflammatory response may give rise to chronic diseases.

Crystalline quartz could induce surface inflammation, increase lung permeability and cause the type II cells to release their plasma membrane components, resulting in progressive damage, while the damage triggered by amorphous ultrafine silica regressed [217]. In this study, ultrafine/fine carbon black did not cause change in lung permeability or induce inflammation. Pan *et al.* [227] also proved recently that pure carbon black did not induce inflammation to human bronchial cells. Nevertheless, when carbon nanoparticles formed adducts with Pb^{2+} and incubated with human lung cells, the expression of the long novel noncoding RNA which is responsible for the regulation of inflammation was depressed. Pb^{2+} does not induce inflammation individually, just like Cr (VI), but it is revealed that the co-existence of these two species in $PM_{2.5}$ caused cytotoxicity in lung cells [228]. The traffic-related PM is also reported to induce inflammation in both lymphocytes and lung cells [229], where the induction effect is stronger for PM with higher PAHs levels [230]. Additionally, the *in vitro* low dose exposure of rat lung to

silica particles for 24 h exhibited inflammatory response [231], while the *in vivo* long-term, repeated and high-concentration diesel exhaust exposures of rats showed chronic inflammation [219].

5.2.2. Oxidative Stress

Reactive oxygen species (ROS) are highly reactive and unstable. The accumulation of ROS may lead to the oxidation of cellular components when the level is beyond the elimination ability of antioxidants [232], giving rise to oxidative stress. Oxidative stress may cause many chronic diseases, such as cancer, diabetics, cardiovascular diseases, and other degenerative diseases [233]. The exposure to PM would lead to oxidative stress to lipids, proteins, and DNA. When PM readily interacts with lung surfactant and penetrates through the membrane to interstitium and epithelial cells, the surface of toxic particles (e.g., metallic particles as catalysts) and the adsorbates including transition metals (copper, iron and manganese, etc.) and PAHs can generate free radicals to cause oxidative stress. Additionally, the mechanical damage brought about by PM within the cells could also trigger oxidative stress [234].

It is found that the presence of traffic-related PM led to an increase of ROS generation and oxidative DNA damage in human lymphocytes, alveolar epithelial adenocarcinoma cells [229], and type II lung epithelial A549 cells [235]. The extent of oxidative stress, cytotoxicity and epithelial activation on pulmonary cells induced by diesel exhaust particles increased with the content of PAHs [230]. Soltani *et al.* [236] investigated the influence of TiO_2 and Fe_2O_3 micro and nanoparticles on lung and marrow tissues, figuring out that the particles increased the baseline level of lipid oxidation and antioxidant enzyme activity. The toxicity caused by TiO_2 nanoparticles was more serious than that caused by the microparticles and the Fe_2O_3 nanoparticles. The acute induction of oxidative damage can also be observed with *in vivo* study. The Superoxide Dismutase (SOD) activity in rats was reduced after the exposure of the rats to ambient PM, which indicates the oxidative stress caused by the particles [237].

Besides lung cells, it is also reported that PM may aggravate oxidative stress in kidney. The *in vitro* exposure of human kidney cells to traffic-related particles indicated that the particles reduced the viability of the cells, increased mitochondrial ROS and decreased mitochondrial membrane potential, which led to kidney disease [238].

5.2.3. Other Adverse Health Effects of PM

In addition to inflammation and oxidative damage responses, PM is also associated with many other toxicity and diseases. Silver nanoparticles were discovered to induce autophagy and apoptosis in mouse embryonic fibroblast cells [239] and cytotoxicity in human lung cells [240]. The *in vivo* study on mice lasting for one month proved that PM is the initiator of pulmonary fibrosis since lung inflammation and incipient fibrosis symptoms were discovered after the exposure [241]. For susceptible rats with hypertension, the heart rate and heart rate variability were found linked to the industrial exhaust [242]. The short-term *in vivo* studies of humans revealed that ambient $PM_{2.5}$ was related to low resting cerebrovascular flow velocity and high resting cerebrovascular resistance, suggesting that the endothelial function in the cerebral vasculature would be harmed by $PM_{2.5}$ [243].

The pathological symbols, such as chronic inflammation, increased mucus and phospholipids production, that are exhibited by patients with chronic obstructive pulmonary diseases would be aggravated with time and PM concentration. However, in the chronic study on young and normal rats, the pathological symbols remained stable after 12-18 months of exposure to PM of medium and high concentrations. It implied that young and normal rats were resistant to chronic diesel exhaust exposures [219]. Recent papers discussing long-term *in vivo* studies presented some new physiological responses upon exposure to PM. Lepeule *et al.* [244] reported that the traffic particles (mostly carbon black) caused an additional rate of decline in forced vital capacity and forced expiratory volume, which indicated a lower baseline lung function. The particles also

accelerated the decline of lung function in the elderly. PM can affect the function of other organs as well. Liang *et al.* [245] let the rats be exposed to PM$_{2.5}$ once every three days for one month. Then the rats got vascular endothelial injury and inflammation, and meanwhile, fibrin thrombi and bleeding occurred on the lung tissue. All of these responses suggest that PM$_{2.5}$ would eventually lead to disseminated intravascular coagulation. Long-term gasoline vehicle exhaust exposure is proved to induce erectile dysfunction in rats [246].

Transgenic mice were used to test with PM samples [247]. After 4 h exposure, it was found that the PM induced the increase of CYP1A1 (a gene regulated by aryl hydrocarbon receptor), which indicated a carcinogenic effect. Besides, PM led to an increase of endothelin-1which exhibited as a dysfunction of epithelial, and an increase of metallothionein-II resulting in reduced scavenging of metal toxicity. The exposure to PM does not cause a widespread change in gene expression. This is consistent with the results of the study on silica particles [231]. PM$_{2.5}$ was only reported to cause oxidative damage to DNA in humans [237]. However, a recent study that exposing zebra to carbon nanoparticles showed a disturbance on DNA methylation of the genes in heart tissue, revealing the unregulated gene expression caused by PM [248].

6. Summary and Perspectives

It is revealed that exposure to PM significantly impacts on pulmonary surfactant and human health through altering the physiological, biophysical and morphological properties of lung surfactant. Different types of particles including synthetic and ambient PM, which are not equally toxic to pulmonary surfactant and health, have been proved by both experimental investigations and molecular dynamics simulations. It has been found that the strength of particle-surfactant interaction increases with the extent of hydrophobicity and surface charge density, while each type of particles bears its own critical particle size that shows the strongest impacts on surfactant. Particle shape and chemical nature of PM also influence the phase behavior and morphology of pulmonary surfactant.

Many different characterizations and methodologies have been used to investigate PM-surfactant interaction. The interpretability of interdisciplinary approaches greatly promotes a comprehensive understanding of the effects of PM. Nevertheless, quantitative analyses of, for example, the interaction forces between particles and lung surfactant, and the surfactant domain change upon the contact with particles, are seldom presented. Future studies of the associated interfacial forces can be carried out with nanomechanical tools such as atomic force microscopy and surface forces apparatus. The effect of PM on the morphology is generally investigated via visual characterization (e.g., AFM, BAM). Further investigation utilizing fluorescence microscope can provide useful information on the morphological changes upon PM deposition. Meanwhile, the continuous monitoring of the change in various properties of lung surfactant after the deposition of PM is mostly reported with molecular dynamics simulations. It would be more convincing with direct and real-time experimental visualization before, during and after the deposition of PM on pulmonary surfactant.

The different results obtained for naturally derived surfactant and DPPC after PM deposition suggest that the functions of other lipids and surface proteins cannot be ignored. Though DPPC is the major component of lung surfactant and responsible for maintaining the phase behavior and stability of alveoli during respiration, the results could be more conclusive when naturally derived surfactant is considered. It is reported that surfactant proteins, especially SP-B, affect the domain change significantly by increasing the line tension and dipole density difference, etc. [147] Future studies of the interactions between PM and lung surfactant in the presence of surfactant proteins will provide useful insights into a more complete understanding of the physiochemical interaction mechanisms.

Synthetic particles are utilized to validate the interaction mechanism because of their known chemical composition, which furthermore provides a guideline for nanotechnology safety. However, the influence of actual ambient PM could not be fully represented by synthetic particles, since the existence of other components in ambient PM interferes with the interaction. Studies on natural PM would give rise to more practical and environmentally relevant information. Meanwhile, the composition of PM varies with time and location, but the research about how different environmentally derived PM affects the phase behavior of lung surfactant is still lacking. In some literature, the concentrations of PM used are much higher than the actual exposure dose. Though this approach is convenient to obtain acute responses, the feasibility of the inference on the actual health effect should be noted.

The studies of PM-surfactant interaction are all performed on planar interfaces with the utilization of LB-trough and other imaging instruments. However, the curvature effect of spheric alveoli has been proved to impact the morphology and dynamics of the lung surfactant. Sachan *et al.* [144] found that when the radius of Survanta monolayer-covered bubbles decreased to 100 μm, which is comparable to the size of alveoli, the LC domains changed dramatically from dispersed circles to meshing stripes, separating the original continuous LE matrix to a discontinuous phase. This change comes from the anisotropic bending energy [141,146]. This interfacial curvature effect on the monolayer also leads to changes in surfactant adsorption and the dilatational modulus [144]. The observation resulted from alveoli-sized curvature implies that future investigations of PM-surfactant interaction on curved interfaces could provide more practical information at alveolar dimensions. Instruments such as captive bubble surfactometer, pulsating bubble surfactometer and constrained drop surfactometer can be used to study on curved surfaces. Besides curvature effect, other factors such as temperature and rate of film oscillation also limit the physiological relevance of the *in vitro* studies on surfactant films. Constrained drop surfactometer can be used to investigate the surfactant activity and inhibition under physiologically relevant conditions [198,249]. The surfactant films are constrained in a sessile drop, and the compression and expansion of the droplet are controlled at physiologically relevant rates. This technique has great potential to study PM-surfactant interactions at molecular level to provide insight into the physiochemical effects of PM.

The *in vitro* studies on PM-surfactant interactions provide physical evidence of how PM affects lung surfactant, implying the impairment on physiological properties of lung surfactant. However, the direct mechanisms of how PM induces pulmonary dysfunction physiologically are still unclear since the *in vivo* measurement of the changes in surfactant functions upon PM deposition is challenging. Riva *et al.* [250] conducted an *in vivo* experiment to investigate how lung mechanics changes upon low dose instillation of ambient PM. The elastic and viscoelastic components of lung mechanics were increased, indicating the impaired lung function. The authors attributed this mechanical alteration to the inflammation and oxidative stress caused by the penetration of PM into the alveolar regions. Further experimental evidence is needed to illustrate the correlation between physiological responses and biophysical change.

Although the changes in the biophysical properties of modal or replica lung surfactant under the effect of engineered NPs and some environmental PM$_{2.5}$ have been investigated, correlating *in vitro* studies with the *in vivo* systems still remains a challenge. Biological relevant surfactant models integrating natural surfactant components and monolayer, bilayer and multilayer structures are required to study the PM-surfactant interaction. A number of studies on PM and naturally derived surfactant have been conducted, as well as the investigations of PM on bilayer and multilayer structures. Future studies between PM and complex surfactant structures using techniques that can mimic

physiological conditions are still needed. Moreover, the use of environmental $PM_{2.5}$ in addition to engineered nanoparticles is beneficial to evaluating the actual effects of air pollutants. Though the biophysical *in vitro* studies provide a good implication of PM-induced health effects, the physiological studies directly related to the biophysical changes are still lacking. It is noted that non-equilibrium state may exist due to the relative humidity gradient in the alveolar space, giving rise to disparity in the composition and layered structures of lung surfactant at the interface. This thermodynamic condition should be considered when studying the structures of the multilayered films [251].

There is a big concern that even though the PM pollution is within the range of Environmental Protection Agency annual air quality standards, the long-term exposure still causes adverse health effects [244,252]. This observation is an implication to governmental actions that appropriate and strict regulations should be complemented according to the discrepancies on different types of PM and chronic effects.

Declaration of Competing Interest

The authors declare that they have no known competing financial interests or personal relationships that could have appeared to influence the work reported in this paper.

Acknowledgements

References

[1] Brook RD, Rajagopalan S, Pope III CA, Brook JR, Bhatnagar A, Diez-Roux AV, et al. Circulation 2010;121:2331–78. https://doi.org/10.1161/CIR.0b013e3181dbece1.
[2] Pope III CA, Dockery DW. J Air Waste Manage Assoc 2006;56:709–42. https://doi.org/10.1080/10473289.2006.10464485.
[3] WHO. WHO Air quality guidelines for particulate matter, ozone, nitrogen dioxide and sulfur dioxide: global update 2005: summary of risk assessment. Switzerland: World Health Organization: Geneva; 2006.
[4] Sundeep S, Anders B, Bertil R, Frank K, Thomas S, Stephen TH, et al. Am J Respir Crit Care Med 1999;159:702–9. https://doi.org/10.1164/ajrccm.159.3.9709083.
[5] Laden F, Schwartz J, Speizer FE, Dockery DW. Am J Respir Crit Care Med 2006;173:667–72. https://doi.org/10.1164/rccm.200503-443OC.
[6] Dockery DW, Pope CA, Xu X, Spengler JD, Ware JH, Fay ME, et al. N Engl J Med 1993;329:1753–9. https://doi.org/10.1056/nejm199312093292401.
[7] Miller KA, Siscovick DS, Sheppard L, Shepherd K, Sullivan JH, Anderson GL, et al. N Engl J Med 2007;356:447–58. https://doi.org/10.1056/NEJMoa054409.
[8] Brain JD, Valberg PA. Am Rev Respir Dis 1979;120:1325–73. https://doi.org/10.1164/arrd.1979.120.6.1325.
[9] Usmani OS, Biddiscombe MF, Barnes PJ. Am J Respir Crit Care Med 2005;172:1497–504. https://doi.org/10.1164/rccm.200410-1414OC.
[10] Zhang Q, He K, Huo H. Nature 2012;484:161. https://doi.org/10.1038/484161a.
[11] Cormier Stephania A, Lomnicki S, Backes W, Dellinger B. Environ Health Perspect 2006;114:810–7. https://doi.org/10.1289/ehp.8629.
[12] Mitchell DM, Solomon MA, Tolfree SE, Short M, Spiro SG. Thorax 1987;42:457. https://doi.org/10.1136/thx.42.6.457.
[13] Oberdörster G, Oberdörster E, Oberdörster J. Environ Health Perspect 2005;113:823–39. https://doi.org/10.1289/ehp.7339.
[14] Jayaratne ER, Clifford S, Morawska L. Environ Sci Technol 2015;49:12751–7. https://doi.org/10.1021/acs.est.5b01851.
[15] Zhang XY, Wang YQ, Niu T, Zhang XC, Gong SL, Zhang YM, et al. Atmos Chem Phys 2012;12:779–99. https://doi.org/10.5194/acp-12-779-2012.
[16] Wang YQ, Zhang XY, Sun JY, Zhang XC, Che HZ, Li Y. Atmos Chem Phys 2015;15:13585–98. https://doi.org/10.5194/acp-15-13585-2015.
[17] Che H, Zhao H, Wu Y, Xia X, Zhu J, Wang H, et al. Meteorog Atmos Phys 2015;127:345–54. https://doi.org/10.1007/s00703-015-0367-3.
[18] Tainio M, Juda-Rezler K, Reizer M, Warchałowski A, Trapp W, Skotak K. Reg Environ Chang 2013;13:705–15. https://doi.org/10.1007/s10113-012-0366-6.
[19] Wang X, Dickinson RE, Su L, Zhou C, Wang K. Bull Am Meteorol Soc 2018;99:105–19. https://doi.org/10.1175/bams-d-16-0301.1.
[20] Kim K-H, Kabir E, Kabir S. Environ Int 2015;74:136–43. https://doi.org/10.1016/j.envint.2014.10.005.
[21] Rao X, Zhong J, Brook RD, Rajagopalan S. Antioxid Redox Signal 2018;28:797–818. https://doi.org/10.1089/ars.2017.7394.
[22] Liu H-Y, Dunea D, Iordache S, Pohoata A. Atmosphere 2018;9:150. https://doi.org/10.3390/atmos9040150.
[23] Mühlfeld C, Rothen-Rutishauser B, Blank F, Vanhecke D, Ochs M, Gehr P. Am J Phys Lung Cell Mol Phys 2008;294:L817–29. https://doi.org/10.1152/ajplung.00442.2007.
[24] Schleh C, Hohlfeld JM. Inhal Toxicol 2009;21:97–103. https://doi.org/10.1080/08958370903005744.
[25] Garcia-Mouton C, Hidalgo A, Cruz A, Pérez-Gil J. Eur J Pharm Biopharm 2019;144:230–43. https://doi.org/10.1016/j.ejpb.2019.09.020.
[26] Hidalgo A, Cruz A, Pérez-Gil J. Biochim Biophys Acta Biomembr 2017;1859:1740–8. https://doi.org/10.1016/j.bbamem.2017.04.019.
[27] Hidalgo A, Cruz A, Pérez-Gil J. Eur J Pharm Biopharm 2015;95:117–27. https://doi.org/10.1016/j.ejpb.2015.02.014.
[28] Kundu S, Stone EA. Environ. Sci: Processes Impacts 2014;16:1360–70. https://doi.org/10.1039/c3em00719g.
[29] Snider G, Weagle CL, Murdymootoo KK, Ring A, Ritchie Y, Stone E, et al. Atmos Chem Phys 2016;16:9629. https://doi.org/10.5194/acp-16-9629-2016.
[30] Dominici WF, Wang AY, Correia WA, Ezzati WM, Pope WC, Dockery WD. Epidemiology 2015;26:556–64. https://doi.org/10.1097/EDE.0000000000000297.
[31] Li N, Sioutas C, Cho A, Schmitz D, Misra C, Sempf J, et al. Environ Health Perspect 2003;111:455–60. https://doi.org/10.1289/ehp.6000.
[32] White A, Bradshaw P, Herring A, Teitelbaum S, Beyea J, Stelman SD, et al. Cancer Res 2016;76. https://doi.org/10.1158/1538-7445.SABCS15-P6-09-08.
[33] Motorykin O, Matzke MM, Waters K, Simonich S. Environ Sci Technol 2013;47:3410–6. https://doi.org/10.1021/es305295d.
[34] Hou J, Sun H, Huang X, Zhou Y, Zhang Y, Yin W, et al. Chemosphere 2017;185:1136–43. https://doi.org/10.1016/j.chemosphere.2017.07.056.
[35] Liu L, Dong F, He X, Dai Q, Huang Y. Key Eng Mater 2013;562-565:1434–9. https://doi.org/10.4028/www.scientific.net/KEM.562-565.1434.
[36] Bond TC, Streets DG, Yarber KF, Nelson SM, Woo JH, Klimont Z. J Geophys Res-Atmos 2004;109. https://doi.org/10.1029/2003JD003697 n/a-n/a.
[37] James JS. J Expo Anal Environ Epidemiol 2003;13:443. https://doi.org/10.1038/sj.jea.7500298.
[38] Dai Q, Bi X, Song W, Li T, Liu B, Ding J, et al. Atmos Environ 2019;196:66. https://doi.org/10.1016/j.atmosenv.2018.10.002.
[39] Wang W, Wang S, Xu J, Zhou R, Shi C, Zhou B. Environ Sci Pollut Res 2016;23:1691–702. https://doi.org/10.1007/s11356-015-5397-3.
[40] Shen J, Liu X, Zhang Y, Fangmeier A, Goulding K, Zhang F. Atmos Environ 2011;45:5033–41. https://doi.org/10.1016/j.atmosenv.2011.02.031.
[41] Han X, Guo Q, Liu C, Fu P, Strauss H, Yang J, et al. Tian L. Sci Rep 2016;6. https://doi.org/10.1038/srep29958.
[42] Han X, Guo Q, Strauss H, Liu C, Hu J, Guo Z, et al. Environ Sci Technol 2017;51:7794–803. https://doi.org/10.1021/acs.est.7b00280.
[43] Zhang Q, Streets DG, Carmichael G, He K, Huo H, Kannari A, et al. Atmos Chem Phys 2009;9:5131–53. https://doi.org/10.5194/acp-9-5131-2009.
[44] Tai APK, Mickley LJ, Jacob DJ. Atmos Environ 2010;44:3976–84. https://doi.org/10.1016/j.atmosenv.2010.06.060.
[45] Kim YH, Krantz QT, McGee J, Kovalcik KD, Duvall RM, Willis RD, et al. Environ Pollut 2016;218:1180–90. https://doi.org/10.1016/j.envpol.2016.08.073.
[46] Maynard AD, Aitken RJ, Butz T, Colvin V, Donaldson K, Oberdörster G, et al. Nature 2006;444:267–9. https://doi.org/10.1038/444267a.
[47] Kipen HM, Laskin DL. Am J Phys Lung Cell Mol Phys 2005;289:L696–7. https://doi.org/10.1152/ajplung.00277.2005.
[48] Veldhuizen R, Nag K, Orgeig S, Possmayer F. Biochim Biophys Acta (BBA) - Mol Basis Dis 1998;1408:90–108. https://doi.org/10.1016/S0925-4439(98)00061-1.
[49] In Possmayer F, Polin RA, Fox WW, Abman SH. Fetal and Neonatal Physiology (Third Edition). , Vol. 2W. B. Saunders Company; 2004; 1014–34. https://doi.org/10.1016/B978-0-7216-9654-6.50104-1 Chapter 101.
[50] Rugonyi S, Biswas SC, Hall SB. Respir Physiol Neurobiol 2008;163:244–55. https://doi.org/10.1016/j.resp.2008.05.018.
[51] Han S, Mallampalli RK. Ann Am Thorac Soc 2015;12:765–74. https://doi.org/10.1513/AnnalsATS.201411-507FR.
[52] Johansson J, Curstedt T. Eur J Biochem 1997;244:675–93. https://doi.org/10.1111/j.1432-1033.1997.00675.x.
[53] Hartshorn KL, Crouch EC, White MR, Eggleton P, Tauber AI, Chang D. Sastry K. J Clin Invest 1994;94:311–9. https://doi.org/10.1172/JCI117323.
[54] Crouch E, Persson A, Chang D. Heuser J. J Biol Chem 1994;269:17311–9.
[55] McCormack F. CHEST 1997;111:114S–9S. https://doi.org/10.1378/chest.111.6_Supplement.114S.
[56] Voss T, Eistetter H, Schäfer KP, Engel J. J Mol Biol 1988;201:219–27. https://doi.org/10.1016/0022-2836(88)90448-2.
[57] Wright JR. Neonatology 2004;85:326–32. https://doi.org/10.1159/000078172.
[58] Chabot S, Koumanov K, Lambeau G, Gelb MH, Balloy V, Chignard M, et al. J Immunol 2003;171:995. https://doi.org/10.4049/jimmunol.171.2.995.
[59] Hawgood S, Derrick M, Poulain F. Biochimica et Biophysica Acta (BBA) - Molecular Basis of Disease, 1408; 1998; 150–60. https://doi.org/10.1016/S0925-4439(98)00064-7.
[60] Pérez-Gil J, Tucker J, Simatos G, Keough KMW. Biochem Cell Biol 1992;70:332–8. https://doi.org/10.1139/o92-051.
[61] Johansson J, Szyperski T, Curstedt T, Wuethrich K. Biochemistry 1994;33:6015–23. https://doi.org/10.1021/bi00185a042.
[62] von Nahmen A, Post A, Galla H-J, Sieber M. Eur Biophys J 1997;26:359–69. https://doi.org/10.1007/s002490050090.

[63] Ding J, Takamoto DY, von Nahmen A, Lipp MM, Lee KYC, Waring AJ, Zasadzinski JA, Biophys. J., 2001; 80: 2262-2272, doi:doi:10.1016/S0006-3495(01)76198-X.

[64] Walther FJ, Waring AJ, Sherman MA, Zasadzinski JA, Gordon LM. Neonatology 2007;91:303–10. https://doi.org/10.1159/000101346.

[65] Lu J, Willis AC, Reid KBM. Biochem J 1992;284:795. https://doi.org/10.1042/bj2840795.

[66] Ikegami M, Hull WM, Yoshida M, Wert SE, Whitsett JA. Am J Phys Lung Cell Mol Phys 2001;281:L697–703. https://doi.org/10.1152/ajplung.2001.281.3.L697.

[67] Hogenkamp A, Herías MV, Tooten PCJ, Veldhuizen EJA, Haagsman HP. Mol Immunol 2007;44:3517–27. https://doi.org/10.1016/j.molimm.2007.03.013.

[68] Numata M, Kandasamy P, Voelker DR. Expert Rev Respir Med 2012;6:243–6. https://doi.org/10.1586/ers.12.21.

[69] Piknova B, Schram V, Hall S. Curr Opin Struct Biol 2002;12:487–94. https://doi.org/10.1016/S0959-440X(02)00352-4.

[70] Goerke J, Gonzales J. J Appl Physiol 1981;51:1108–14. https://doi.org/10.1152/jappl.1981.51.5.1108.

[71] Davis PJ, Fleming BD, Coolbear KP, Keough KMW. Biochemistry 1981;20:3633–6. https://doi.org/10.1021/bi00515a051.

[72] Pérez-Gil J. Biochim Biophys Acta Biomembr 2008;1778:1676–95. https://doi.org/10.1016/j.bbamem.2008.05.003.

[73] Bernhard W, Hoffmann S, Dombrowsky H, Rau GA, Kamlage A, Kappler M, et al. Am J Respir Cell Mol Biol 2001;25:725–31. https://doi.org/10.1165/ajrcmb.25.6.4616.

[74] Bernhard W. Annals of Anatomy - Anatomischer Anzeiger 2016;208:146–50. https://doi.org/10.1016/j.aanat.2016.08.003.

[75] Gille C, Spring B, Bernhard W, Gebhard C, Basile D, Lauber K, et al. J Lipid Res 2007;48:307–17. https://doi.org/10.1194/jlr.M600451-JLR200.

[76] Korchowiec B, Stachowicz-Kuśnierz A, Korchowiec J. Environ Sci: Processes & Impacts 2019;21:438–45. https://doi.org/10.1039/C8EM00497H.

[77] Kandasamy P, Zarini S, Chan ED, Leslie CC, Murphy RC, Voelker DR. J Biol Chem 2011;286:7841–53. https://doi.org/10.1074/jbc.M110.170241.

[78] Fessler MB, Summer RS. Am J Respir Cell Mol Biol 2016;54:624–35. https://doi.org/10.1165/rcmb.2016-0011PS.

[79] Klenz U, Saleem M, Meyer MC, Galla HJ. Biophys J 2008;95:699–709. https://doi.org/10.1529/biophysj.108.131102.

[80] Nishiura A, Murakami T, Higashi Y, Yata N. Pharm Res 1988;5:209–13. https://doi.org/10.1023/a:1015985511653.

[81] Agassandian M, Mallampalli RK, Biochimica et Biophysica Acta (BBA) - Molecular and Cell Biology of Lipids, 2013; 1831: 612-625, doi:doi:10.1016/j.bbalip.2012.09.010.

[82] Birner R, Bürgermeister M, Schneiter R, Daum G. Mol Biol Cell 2001;12:997–1007. https://doi.org/10.1091/mbc.12.4.997.

[83] Dowhan W, Bogdanov M. Annu Rev Biochem 2009;78:515–40. https://doi.org/10.1146/annurev.biochem.77.060806.091251.

[84] Kooijman EE, Kuzenko SR, Gong D, Best MD, Folkesson HG. Am J Phys Lung Cell Mol Phys 2011;301:L804–11. https://doi.org/10.1152/ajplung.00445.2010.

[85] Orgeig S, Daniels CB. Comparative Biochemistry and Physiology Part A: Molecular & Integrative Physiology, 129; 2001; 75–89. https://doi.org/10.1016/S1095-6433(01)00307-5.

[86] Postle AD, Heeley EL, Wilton DC. Comp Biochem Physiol A Mol Integr Physiol 2001;129:65–73. https://doi.org/10.1016/S1095-6433(01)00306-3.

[87] Creuwels LAJM, van Golde LMG, Haagsman HP. Lung 1997;175:1–39. https://doi.org/10.1007/PL00007554.

[88] Jackson JC, Gleason CA, Juul SE. Avery's Diseases of the Newborn (Tenth Edition). Elsevier; 2018; 653–67. https://doi.org/10.1016/B978-0-323-40139-5.00046-2.

[89] Zasadzinski JA, Stenger PC, Shieh I, Dhar P. Biochimica et Biophysica Acta (BBA) - Biomembranes, 1798; 2010; 801–28. https://doi.org/10.1016/j.bbamem.2009.12.010.

[90] Lopez-Rodriguez E, Pérez-Gil J. Biochim Biophys Acta Biomembr 2014;1838:1568–85. https://doi.org/10.1016/j.bbamem.2014.01.028.

[91] Bangham AD, Morley CJ, Phillips MC. Biochim Biophys Acta 1979;573:552–6. https://doi.org/10.1016/0005-2760(79)90229-7.

[92] Pérez-Gil J, Keough KMW. Biochim Biophys Acta (BBA) - Mol Basis Dis 1998;1408:203–17. https://doi.org/10.1016/S0925-4439(98)00068-4.

[93] Piknova B, Schief WR, Vogel V, Discher BM, Hall SB. Biophys J 2001;81:2172–80. https://doi.org/10.1016/S0006-3495(01)75865-1.

[94] Yan W, Piknova B, Hall SB. Biophys J 2005;89:306–14. https://doi.org/10.1529/biophysj.105.060947.

[95] Discher BM, Schief WR, Vogel V, Hall SB. Biophys J 1999;77:2051–61. https://doi.org/10.1016/S0006-3495(99)77046-3.

[96] Guzmán E, Santini E, Ferrari M, Liggieri L, Ravera F. Langmuir 2017;33:10715–25. https://doi.org/10.1021/acs.langmuir.7b02484.

[97] Konduru NV, Damiani F, Stoilova-McPhie S, Tresback JS, Pyrgiotakis G, Donaghey TC, et al. Langmuir 2018;34:6454–61. https://doi.org/10.1021/acs.langmuir.7b03741.

[98] Dobrowolska K, Jabłczyńska K, Kondej D. Sosnowski TR 2018;54. https://doi.org/10.5277/ppmp1837.

[99] Hao C, Li J, Mu W, Zhu L, Yang J, Liu H, et al. Appl Surf Sci 2016;362:121–5. https://doi.org/10.1016/j.apsusc.2015.11.173.

[100] Kadoya C, Lee B-W, Ogami A, Oyabu T. Nishi K-i, Yamamoto M, Todoroki M, Morimoto Y, Tanaka I, Myojo T. Nanotoxicology 2016;10:194–203. https://doi.org/10.3109/17435390.2015.1039093.

[101] Mousseau F, Berret JF. Soft Matter 2018;14:5764–74. https://doi.org/10.1039/c8sm00925b.

[102] Mousseau F, Le Borgne R, Seyrek E, Berret JF. Langmuir 2015;31:7346–54. https://doi.org/10.1021/acs.langmuir.5b01639.

[103] Harishchandra RK, Saleem M, Galla H-J. J R Soc Interface 2010;7:15–26. https://doi.org/10.1098/rsif.2009.0329.focus.

[104] Beck-Broichsitter M. Langmuir 2016;32:10422–9. https://doi.org/10.1021/acs.langmuir.6b02893.

[105] Beck-Broichsitter M. Langmuir 2018;34:540–5. https://doi.org/10.1021/acs.langmuir.7b03818.

[106] Zhang K, Liu L, Bai T, Guo Z. J Biomed Nanotechnol 2018;14:526–35. https://doi.org/10.1166/jbn.2018.2497.

[107] Bakshi MS, Zhao L, Smith R, Possmayer F, Petersen NO. Biophys J 2008;94:855–68. https://doi.org/10.1529/biophysj.107.106971.

[108] Tatur S, Badia A. Langmuir 2012;28:628–39. https://doi.org/10.1021/la203439u.

[109] Zhao Q, Li Y, Chai X, Zhang L, Xu L, Huang J, et al. Chemosphere 2019;215:746–52. https://doi.org/10.1016/j.chemosphere.2018.10.016.

[110] Sosnowski TR, Koliński M, Gradoń L. Ann Occup Hyg 2011;55:329–38. https://doi.org/10.1093/annhyg/mer007.

[111] Padilla-Chavarra HI, Guizado TRC, Pimentel AS. Phys Chem Chem Phys 2015;17:20912–22. https://doi.org/10.1039/c5cp01443c.

[112] Stachowicz-Kuśnierz A, Trojan S, Cwiklik L, Korchowiec B, Korchowiec J. Chem Eur J 2017;23:5307–16. https://doi.org/10.1002/chem.201605945.

[113] Matyszewska D, Tappura K, Orädd G, Bilewicz R. J Phys Chem B 2007;111:9908–18. https://doi.org/10.1021/jp068874g.

[114] Kanishtha T, Banerjee R, Venkataraman C. Environ Toxicol Pharmacol 2006;22:325–33. https://doi.org/10.1016/j.etap.2006.05.003.

[115] Kendall M. Am J Phys Lung Cell Mol Phys 2007;293:L1053. https://doi.org/10.1152/ajplung.00131.2007.

[116] Kaganer VM, Möhwald H, Dutta P. Rev Mod Phys 1999;71:779–819. https://doi.org/10.1103/RevModPhys.71.779.

[117] Nandi N, Vollhardt D. Chem Rev 2003;103:4033–76. https://doi.org/10.1021/cr0006674.

[118] Leite FL, Bueno CC, Da Róz AL, Ziemath EC. Oliveira ON. Int J Mol Sci 2012;13. https://doi.org/10.3390/ijms131012773.

[119] Hamaker HC. Physica 1937;4:1058–72. https://doi.org/10.1016/S0031-8914(37)80203-7.

[120] van der Wel C, Heinrich D, Kraft DJ. Biophys J 2017;113:1037–46. https://doi.org/10.1016/j.bpj.2017.07.019.

[121] Danov K, Aust R, Durst F, Lange U. J Colloid Interface Sci 1995;175:36–45. https://doi.org/10.1006/jcis.1995.1426.

[122] Dimova R, Dietrich C, Hadjiisky A, Danov K, Pouligny B. The European Physical Journal B - Condensed Matter and Complex Systems 1999;12:589–98. https://doi.org/10.1007/s100510051042.

[123] Barrow RE, Hills BA. J Physiol 1979;295:217–27. https://doi.org/10.1113/jphysiol.1979.sp012963.

[124] Ulman A. An Introduction to Ultrathin Organic Films: From Langmuir–Blodgett to Self–Assembly. Academic Press; 1991. https://doi.org/10.1016/C2009-0-22306-3 Chapter Chapter.

[125] Rubinger CPL, Moreira RL, Cury LA, Fontes GN, Neves BRA, Meneguzzi A, et al. Appl Surf Sci 2006;253:543–8. https://doi.org/10.1016/j.apsusc.2005.12.096.

[126] Chimote G, Banerjee R. Respir Physiol Neurobiol 2005;145:65–77. https://doi.org/10.1016/j.resp.2004.10.003.

[127] Behyan S, Borozenko O, Khan A, Faral M, Badia A, Dewolf C. Environ. Sci: Nano 2018;5:1218–30. https://doi.org/10.1039/c8en00189h.

[128] Matyszewska D, Bilewicz R, Annales UMCS. Chemia 2008;63:201–10. https://doi.org/10.2478/v10063-009-0009-z.

[129] Kondej D, Sosnowski T. Environ Sci Pollut Res 2016;23:4660–9. https://doi.org/10.1007/s11356-015-5610-4.

[130] Kodama Akihisa T, Kuo C-C, Boatwright T, Dennin M. Biophys J 2014;107:1573–81. https://doi.org/10.1016/j.bpj.2014.08.010.

[131] Farnoud AM. Fiegel. J J Aaerosol Med Pulmon Drug Deliv 2016;29:10–23. https://doi.org/10.1089/jamp.2014.1165.

[132] Ma G, Allen HC. Langmuir 2006;22:5341–9. https://doi.org/10.1021/la0535227.

[133] Alonso C, Alig T, Yoon J, Bringezu F, Warriner H, Zasadzinski JA. Biophysical Journal 2004;87:4188–202. https://doi.org/10.1529/biophysj.104.051201.

[134] Farnoud AM, Fiegel J. J Phys Chem B 2013;117:12124–34. https://doi.org/10.1021/jp405924y.

[135] Wüstneck R, Perez-Gil J, Wüstneck N, Cruz A, Fainerman VB, Pison U. Adv Colloid Interf Sci 2005;117:33–58. https://doi.org/10.1016/j.cis.2005.05.001.

[136] Wüstneck N, Wüstneck R, Fainerman VB, Miller R, Pison U. Colloids Surf B: Biointerfaces 2001;21:191–205. https://doi.org/10.1016/S0927-7765(01)00172-2.

[137] Enhorning G. Comparative Biochemistry and Physiology Part A: Molecular & Integrative Physiology 2001;129:221–6. https://doi.org/10.1016/S1095-6433(01)00318-X.

[138] Zuo YY, Ding M, Bateni A, Hoorfar M, Neumann AW. Colloids Surf A Physicochem Eng Asp 2004;250:233–46. https://doi.org/10.1016/j.colsurfa.2004.04.081.

[139] Hui SW, Viswanathan R, Zasadzinski JA. Israelachvlic JN. Biophys J 1995;68:171–8. https://doi.org/10.1016/S0006-3495(95)80172-4.

[140] McConnell HM, Keller DJ. Proc Natl Acad Sci 1987;84:4706. https://doi.org/10.1073/pnas.84.14.4706.

[141] McConnell HM. Annu Rev Phys Chem 1991;42:171–95. https://doi.org/10.1146/annurev.pc.42.100191.001131.

[142] Seul M, Andelman D. Science 1995;267:476. https://doi.org/10.1126/science.267.5197.476.

[143] McConnell HM, Moy VT. J Phys Chem 1988;92:4520–5. https://doi.org/10.1021/j100326a053.

[144] Sachan AK, Zasadzinski JA. Proc Natl Acad Sci 2018;115:E134. https://doi.org/10.1073/pnas.1715830115.

[145] Ding J, Warriner HE, Zasadzinski JA. Phys Rev Lett 2002;88:168102. https://doi.org/10.1103/PhysRevLett.88.168102.

[146] Sachan AK, Choi SQ, Kim KH, Tang Q, Hwang L, Lee KYC, et al. Soft Matter 2017;13:1481–92. https://doi.org/10.1039/C6SM02797K.

[147] Dhar P, Eck E, Israelachvili JN, Lee DW, Min Y, Ramachandran A, et al. Zasadzinski JA. Biophys J 2012;102:56–65. https://doi.org/10.1016/j.bpj.2011.11.4007.

[148] Zeng H, Hwang DS, Israelachvili JN, Waite JH. Proc Natl Acad Sci 2010;107:12850. https://doi.org/10.1073/pnas.1007416107.

[149] Israelachvili JN. Journal of Colloid and Interface Science 1973;44:259–72. https://doi.org/10.1016/0021-9797(73)90218-X.

[150] Israelachvili A, Israelachvili JN. Intermolecular and Surface Forces (Third Edition). Academic Press; 2011; 223–52. https://doi.org/10.1016/B978-0-12-375182-9.10012-0.

[151] Israelachvili JN, Adams GE. Nature 1976;262:774–6. https://doi.org/10.1038/262774a0.

[152] Israelachvili J, Min Y, Akbulut M, Alig A, Carver G, Greene W, et al. Rep Prog Phys 2010;73:036601. https://doi.org/10.1088/0034-4885/73/3/036601.

[153] Zeng H, Tian Y, Anderson TH, Tirrell M, Israelachvili JN. Langmuir 2008;24:1173–82. https://doi.org/10.1021/la7017242.

[154] Faghihnejad A, Zeng H. Langmuir 2013;29:12443–51. https://doi.org/10.1021/la402244h.

[155] Benz M, Gutsmann T, Chen N, Tadmor R, Israelachvili J. Biophysical Journal 2004;86:870–9. https://doi.org/10.1016/S0006-3495(04)74162-4.

[156] Lee DW, Kristiansen K, Donaldson JSH, Cadirov N, Banquy X, Israelachvili JN. Nat Commun 2015;6:7238. https://doi.org/10.1038/ncomms8238.

[157] Jensen TR, Kjaer K. Möbius D, Miller R (editors), Studies in Interface Science, Vol. 11. Elsevier; 2001. p. 205-254. doi:doi:10.1016/S1383-7303(01)80028-4.

[158] Thomas RK, Penfold J. Langmuir 2015;31:7440–56. https://doi.org/10.1021/la504952k.

[159] Chen Y-T, Su H-S, Hung C-H, Yang P-W, Hu Y, Lin T-L, et al. Langmuir 2017;33:10886–97. https://doi.org/10.1021/acs.langmuir.7b01559.

[160] Stenger PC, Wu G, Miller CE, Chi EY, Frey SL, Lee KYC, et al. Biophys J 2009;97:777–86. https://doi.org/10.1016/j.bpj.2009.05.017.

[161] Li P, Penfold J, Thomas RK, Xu H. Advances in Colloid and Interface Science 2019;269:43–86. https://doi.org/10.1016/j.cis.2019.04.002.

[162] Follows D, Tiberg F, Thomas RK, Larsson M. Biochimica et Biophysica Acta (BBA) - Biomembranes 2007;1768:228–35. https://doi.org/10.1016/j.bbamem.2006.10.004.

[163] Chen X, Wang J, Kristalyn CB, Chen Z. Biophys J 2007;93:866–75. https://doi.org/10.1529/biophysj.106.099739.

[164] Jyoti A, Prokop RM, Li J, Vollhardt D, Kwok DY, Miller R, et al. Colloids and Surfaces A: Physicochemical and Engineering Aspects 1996;116:173–80. https://doi.org/10.1016/0927-7757(96)03589-3.

[165] Dwivedi Mridula V, Harishchandra Rakesh K, Koshkina O, Maskos M, Galla H-J. Biophysical Journal 2014;106:289–98. https://doi.org/10.1016/j.bpj.2013.10.036.

[166] Baoukina S, Rozmanov D, Mendez-Villuendas E, Tieleman DP. Biophysical Journal 2014;107:1136–45. https://doi.org/10.1016/j.bpj.2014.05.053.

[167] Phan MD, Lee J, Shin K. Journal of Oleo Science 2016;65:385–97. https://doi.org/10.5650/jos.ess15261.

[168] Kuo C-C, Kodama AT, Boatwright T, Dennin M. Langmuir 2012;28:13976–83. https://doi.org/10.1021/la301543y.

[169] Kondej D, Sosnowski T. Journal of Nanomaterials 2019;2019. https://doi.org/10.1155/2019/9457683.

[170] Pérez-Gil J, Nag K, Taneva S, Keough KM. Biophysical Journal 1992;63:197–204. https://doi.org/10.1016/S0006-3495(92)81582-5.

[171] Rose D, Rendell J, Lee D, Nag K, Booth V. Biophysical Chemistry 2008;138:67–77. https://doi.org/10.1016/j.bpc.2008.08.006.

[172] Casals C, Cañadas O. Biochimica et Biophysica Acta (BBA) - Biomembranes 2012;1818:2550–62. https://doi.org/10.1016/j.bbamem.2012.05.024.

[173] Curtis EM, Bahrami AH, Weikl TR, Hall CK. Nanoscale 2015;7:14505–14. https://doi.org/10.1039/c5nr02255j.

[174] Ruge CA, Schaefer UF, Herrmann J, Kirch J, Cañadas O, Echaide M, et al. PLoS One 2012;7:e40775. https://doi.org/10.1371/journal.pone.0040775.

[175] Liu B, Hoopes MI, Karttunen M. J Phys Chem B 2014;118:11723–37. https://doi.org/10.1021/jp5050892.

[176] Anderson DS, Patchin ES, Silva RM, Uyeminami DL, Sharmah A, Guo T, et al. Toxicol Sci 2015;144:366–81. https://doi.org/10.1093/toxsci/kfv005.

[177] Chen Y, Yang Y, Xu B, Wang S, Li B, Ma J, et al. J Environ Sci 2017;62:100–14. https://doi.org/10.1016/j.jes.2017.08.018.

[178] Guzmán E, Liggieri L, Santini E, Ferrari M, Ravera F. Colloids and Surfaces A: Physicochemical and Engineering Aspects 2012;413:280–7. https://doi.org/10.1016/j.colsurfa.2011.11.023.

[179] Ku T, Gill S, Löbenberg R, Azarmi S, Roa W. Prenner EJ. J Nanosci Nanotechnol 2008;8:2971–8. https://doi.org/10.1166/jnn.2008.171.

[180] van der Wel C, Vahid A, Šarić A, Idema T, Heinrich D, Kraft DJ. Sci Rep 2016;6:32825. https://doi.org/10.1038/srep32825.

[181] Kim J, Chankeshwara SV, Thielbeer F, Jeong J, Donaldson K, Bradley M, et al. Nanotoxicology 2016;10:94–101. https://doi.org/10.3109/17435390.2015.1022887.

[182] Beck-Broichsitter M, Ruppert C, Schmehl T, Günther A, Seeger W, Biochimica et Biophysica Acta (BBA) - Biomembranes, 2014; 1838: 474-481, doi:doi:10.1016/j.bbamem.2013.10.016.

[183] Adair JH, Suvaci E, Sindel J. In Buschow KHJ, Cahn RW, Flemings MC, Ilschner B, Kramer EJ, Mahajan S, Veyssière P (editors), Encyclopedia of Materials: Science and Technology (Second Edition), Elsevier; 2001. p. 1-10. doi:https://doi.org/10.1016/B0-08-043152-6/01622-3.

[184] Derjaguin B. Progress in Surface Science 1993;43:1–14. https://doi.org/10.1016/0079-6816(93)90010-S.

[185] Derjaguin B, Landau L. Progress in Surface Science, 43; 1993; 30–59. https://doi.org/10.1016/0079-6816(93)90013-L.

[186] Verwey EJW. J Phys Coll Chem 1947;51:631–6. https://doi.org/10.1021/j150453a001.

[187] Leite FL, Borato CE, da Silva WTL, Herrmann PSP, Oliveira ON, Mattoso LHC. Microsc Microanal 2007;13:304–12. https://doi.org/10.1017/S1431927607070262.

[188] Israelachvili JN. Intermolecular and Surface Forces (Third Edition). Academic Press; 2011; 291–340. https://doi.org/10.1016/B978-0-12-391927-4.10014-3.

[189] Guzmán E, Liggieri L, Santini E, Ferrari M, Ravera F. J Phys Chem C 2011;115:21715–22. https://doi.org/10.1021/jp207713x.

[190] Chen P, Zhang Z, Gu N, Ji M. Mol Simul 2018;44:85–93. https://doi.org/10.1080/08927022.2017.1342118.

[191] Hu G, Jiao D, Shi X, Valle RP, Fan Q, Zuo YY. ACS Nano 2013;7:10525–33. https://doi.org/10.1021/nn4054683.

[192] Chakraborty A, Mucci NJ, Tan ML, Steckley A, Zhang T, Forrest ML, et al. Langmuir 2015;31:5093–104. https://doi.org/10.1021/la504923j.

[193] Xie L, Cui X, Gong L, Chen J. Zeng H. Langmuir 2020. https://doi.org/10.1021/acs.langmuir.9b03573.

[194] Donaldson SH, Lee CT, Chmelka BF, Israelachvili JN. Proc Natl Acad Sci 2011;108:15699. https://doi.org/10.1073/pnas.1112411108.

[195] Chandler D. Nature 2005;437:640–7. https://doi.org/10.1038/nature04162.

[196] Meyer EE, Rosenberg KJ, Israelachvili J. Proc Natl Acad Sci 2006;103:15739. https://doi.org/10.1073/pnas.0606422103.

[197] Guzmán E, Santini E, Ferrari M, Liggieri L, Ravera F. J Phys Chem C 2015;119:21024–34. https://doi.org/10.1021/acs.jpcc.5b07258.

[198] Valle RP, Huang CL, Loo JSC, Zuo YY. ACS Sustain Chem Eng 2014;2:1574–80. https://doi.org/10.1021/sc500100b.

[199] Kumar P, Bohidar HB. Indian J. Exp Biol 2010;48:1037–42. https://doi.org/10.1080/09612025.2011.536396.

[200] Xu Y, Deng L, Ren H, Zhang X, Huang F, Yue T. Phys Chem Chem Phys 2017;19:17568–76. https://doi.org/10.1039/c7cp02548c.

[201] Lin X, Zuo Y. Gu N, Sci. China Mater 2015;58:28–37. https://doi.org/10.1007/s40843-014-0018-5.

[202] Chatterjee N, Flury M. Langmuir 2013;29:7903–11. https://doi.org/10.1021/la4017504.

[203] Aramrak S, Flury M, Harsh JB, Zollars RL, Davis HP. Langmuir 2013;29:5770–80. https://doi.org/10.1021/la400252q.

[204] Yang K, Ma Y-Q. Nat Nanotechnol 2010;5:579–83. https://doi.org/10.1038/nnano.2010.141.

[205] Zhao Q, Li Y, Chai X, Geng Y, Cao Y, Xu L, Zhang L, Huang J, Ning P, Tian S, Chemosphere, 2019; 222: 603-610, doi:doi:10.1016/j.chemosphere.2019.02.002.

[206] Sosnowski TR, Jabłczyńska K, Odziomek M, Schlage WK, Kuczaj AK. Inhal Toxicol 2018;30:159–68. https://doi.org/10.1080/08958378.2018.1478916.

[207] Wang R, Guo Y, Liu H, Chen Y, Shang Y, Liu H, Journal of Colloid and Interface Science, 2018; 519: 186-193, doi:doi:10.1016/j.jcis.2018.02.021.

[208] Beck-Broichsitter M, Bohr A. Nanotoxicology 2019;13:964–76. https://doi.org/10.1080/17435390.2019.1621400.

[209] Beck-Broichsitter M, Bohr A, Ruge CA. Mol Pharm 2017;14:3464–72. https://doi.org/10.1021/acs.molpharmaceut.7b00477.

[210] Oberdörster G. Int Arch Occup Environ Health 2000;74:1–8. https://doi.org/10.1007/s004200000185.

[211] Mukae H, Vincent R, Quinlan K, English D, Hards J, Hogg JC, et al. Am J Respir Crit Care Med 2001;163:201–9. https://doi.org/10.1164/ajrccm.163.1.2002039.

[212] Husain M, Wu D, Saber AT, Decan N, Jacobsen NR, Williams A, et al. Nanotoxicology 2015;9:1013–22. https://doi.org/10.3109/17435390.2014.996192.

[213] Qin T, Zhang F, Zhou H, Ren H, Du Y, Liang S, et al. Zhao J, Xu J. Front Microbiol 2019;10. https://doi.org/10.3389/fmicb.2019.00054.

[214] Woods PS, Doolittle LM, Rosas LE, Joseph LM, Calomeni EP, Davis IC. Am J Phys Lung Cell Mol Phys 2016;311:L1160–9. https://doi.org/10.1152/ajplung.00339.2016.

[215] Rockx B, Kuiken T, Herfst S, Bestebroer T, Lamers MM, Oude Munnink BB, et al. Science (New York, NY) 2020;368:1012–5. https://doi.org/10.1126/science.abb7314.

[216] Schürch S, Gehr P, Im Hof V, Geiser M, Green F. Respiration Physiology 1990;80:17–32. https://doi.org/10.1016/0034-5687(90)90003-H.

[217] Murphy SA, Bérubé KA, Pooley FD, Richards RJ. Life Sciences 1998;62:1789–99. https://doi.org/10.1016/S0024-3205(98)00141-6.

[218] Chauhan SS, Misra UK, Biochemical Pharmacology, 1991; 41: 191-198, doi:doi:10.1016/0006-2952(91)90476-L.

[219] Ishihara Y, Kagawa J. Inhal Toxicol 2003;15:473–92. https://doi.org/10.1080/08958370304464.

[220] Borie R, Danel C, Debray MP, Taille C, Dombret MC, Aubier M, et al. Eur Respir Rev 2011;20:98. https://doi.org/10.1183/09059180.00001311.

[221] Kuang Z, Hao Y, Hwang S, Zhang S, Kim E, Akinbi HT, et al. Mol Microbiol 2011;79:1220–35. https://doi.org/10.1111/j.1365-2958.2010.07516.x.

[222] Malloy JL, Veldhuizen RAW, Thibodeaux BA, O'Callaghan RJ, Wright JR. Am J Phys Lung Cell Mol Phys 2005;288:L409–18. https://doi.org/10.1152/ajplung.00322.2004.

[223] Martínez-Calle M, Parra E, Olmeda B, Pérez-Gil J. Biophysical Journal 2017;112:503a. https://doi.org/10.1016/j.bpj.2016.11.2723.

[224] Wu Y, Xu Z, Henderson FC, Ryan AJ, Yahr TL, Mallampalli RK. Cell Microbiol 2007;9:1062–72. https://doi.org/10.1111/j.1462-5822.2006.00852.x.

[225] Paunescu A-C, Gabet S, Bougas N, Beydon N, Amat F, Lezmi G, Momas I, Pediatr. Allergy Immunol., 2019; 0, doi:https://doi.org/10.1111/pai.13064.

[226] Chen L, Deng H, Cui H, Fang J, Zuo Z, Deng J, et al. Oncotarget 2017;9:7204–18. https://doi.org/10.18632/oncotarget.23208.

[227] Pan X, Yuan X, Li X, Gao S, Sun H, Zhou H, et al. Environ Sci Technol 2019;53: 4566–78. https://doi.org/10.1021/acs.est.8b06916.

[228] Jia J, Yuan X, Peng X, Yan B. Ecotoxicology and Environmental Safety 2019;172: 152–8. https://doi.org/10.1016/j.ecoenv.2019.01.073.

[229] Vattanasit U, Navasumrit P, Khadka MB, Kanitwithayanun J, Promvijit J, Autrup H, et al. International Journal of Hygiene and Environmental Health 2014;217: 23–33. https://doi.org/10.1016/j.ijheh.2013.03.002.

[230] Bengalli R, Zerboni A, Marchetti S, Longhin E, Priola M, Camatini M, et al. Toxicology Letters 2019;306:13–24. https://doi.org/10.1016/j.toxlet.2019.01.017.

[231] Brown DM, Kanase N, Gaiser B, Johnston H, Stone V. Toxicol Lett 2014;224:147–56. https://doi.org/10.1016/j.toxlet.2013.10.019.

[232] Wang E, Huang Y, Du Q, Sun Y. Environ Toxicol Pharmacol 2017;52:193–9. https://doi.org/10.1016/j.etap.2017.04.010.

[233] Uttara B, Singh AV, Zamboni P, Mahajan RT. Curr Neuropharmacol 2009;7:65–74. https://doi.org/10.2174/157015909787602823.

[234] Papaharalambus CA, Griendling KK. Trends Cardiovasc Med 2007;17:48–54. https://doi.org/10.1016/j.tcm.2006.11.005.

[235] Jantzen K, Roursgaard M, Desler C, Loft S, Rasmussen LJ, Møller P. Mutagenesis 2012;27:693–701. https://doi.org/10.1093/mutage/ges035.

[236] Soltani A, Kahkhaie KR, Haftcheshmeh SM, Jalali Nezhad AA, Akbar Boojar MM. J Cell Biochem 2019;120:7573–80. https://doi.org/10.1002/jcb.28031.

[237] Ma M, Li S, Jin H, Zhang Y, Xu J, Chen D, et al. Sci Total Environ 2015;526:110. https://doi.org/10.1016/j.scitotenv.2015.04.075.

[238] Hsu Y-H, Chuang H-C, Lee Y-H, Lin Y-F, Chen Y-J, Hsiao T-C, et al. Free Radic Biol Med 2019;135:235–44. https://doi.org/10.1016/j.freeradbiomed.2019.03.008.

[239] Lee Y-H, Cheng F-Y, Chiu H-W, Tsai J-C, Fang C-Y, Chen C-W, et al. Biomaterials 2014;35:4706–15. https://doi.org/10.1016/j.biomaterials.2014.02.021.

[240] Gliga AR, Skoglund S, Odnevall Wallinder I, Fadeel B, Karlsson HL. Particle and Fibre Toxicology 2014;11:11. https://doi.org/10.1186/1743-8977-11-11.

[241] Xu Z, Li Z, Liao Z, Gao S, Hua L, Ye X, et al. Ecotoxicol Environ Saf 2019;171:112–21. https://doi.org/10.1016/j.ecoenv.2018.12.061.

[242] Rohr AC, Kamal A, Morishita M, Mukherjee B, Keeler GJ, Harkema JR, et al. Environ Health Perspect 2011;119:474–80. https://doi.org/10.1289/ehp.1002831.

[243] Wellenius Gregory A, Boyle Luke D, Wilker Elissa H, Sorond Farzaneh A, Coull Brent A, Koutrakis P, et al. Stroke 2013;44:1532–6. https://doi.org/10.1161/STROKEAHA.111.000395.

[244] Johanna L, Augusto AL, Brent C, Petros K, David S, Pantel SV, et al. Am J Respir Crit Care Med 2014;190:542–8. https://doi.org/10.1164/rccm.201402-0350OC.

[245] Liang S, Zhao T, Hu H, Shi Y, Xu Q, Miller MR, et al. Sci Total Environ 2019;663: 245–53. https://doi.org/10.1016/j.scitotenv.2019.01.346.

[246] Zhao S, Wang J, Xie Q, Luo L, Zhu Z, Liu Y, et al. J Sex Med 2019;16:155–67. https://doi.org/10.1016/j.jsxm.2018.12.013.

[247] Thomson EM, Williams A, Yauk CL. Vincent R. Particle and Fibre toxicology 2009;6: 6. https://doi.org/10.1186/1743-8977-6-6.

[248] Zhou W, Tian D, He J, Yan X, Zhao J, Yuan X, et al. J Appl Toxicol 2019;39:322. https://doi.org/10.1002/jat.3721.

[249] Sørli JB, Da Silva E, Bäckman P, Levin M, Thomsen BL, Koponen IK, et al. Am J Respir Cell Mol Biol 2015;54:306–11. https://doi.org/10.1165/rcmb.2015-0294MA.

[250] Riva DR, Magalhães CB, Lopes AA, Lanças T, Mauad T, Malm O, et al. Inhal Toxicol 2011;23:257–67. https://doi.org/10.3109/08958378.2011.566290.

[251] Andersson J, Roger K, Larsson M, Sparr E. ACS Central Science 2018;4:1315–25. https://doi.org/10.1021/acscentsci.8b00362.

[252] Hayes RB, Lim C, Zhang Y, Cromar K, Shao Y, Reynolds HR, et al. Int J Epidemiol 2019. https://doi.org/10.1093/ije/dyz114.